AD-A085 512 LESCHACK ASSOCIATES LTD SILVER SPRING MD F/G 8/12
CORRELATION OF UNDER-ICE ROUGHNESS WITH SATELLITE AND AIRBORNE --ETC(U)
MAY 80 L A LESCHACK N00014-76-C-0757
UNCLASSIFIED TR-2 NL

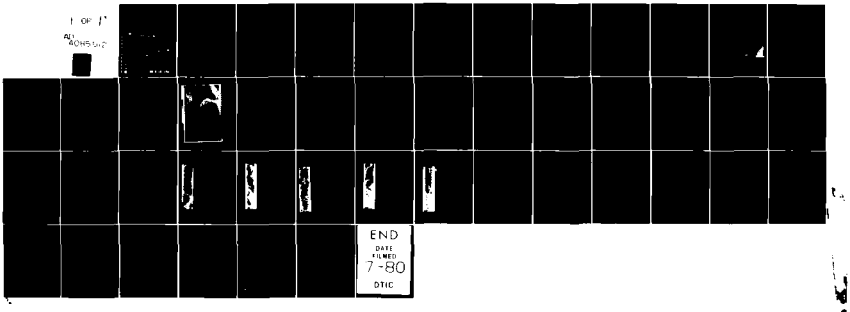

AD A085512

LEVEL II

(12)

(6) CORRELATION OF UNDER-ICE ROUGHNESS WITH SATELLITE AND AIRBORNE THERMAL INFRARED DATA.

by

(10) Leonard A. LeSchack

(11) May 80

(12) 46

(9) Technical report,

(14) TR-2

LeSchack Associates, Ltd.

Suite 116
1111 University Blvd. W.
Silver Spring, Md.
Maryland 20902, U.S.A.
(301) 649-1670

P.O. Box 66
San Ramon,
California 94583, U.S.A.
(415) 649-1077

A Technical Report
Prepared for the
Office of Naval Research

CONTENTS

1. Background 1

2. Under-Ice Roughness 1

3. Preliminary Correlation of RMS Ice Depth with Satellite TIR Temperature Data 7

4. Correlating SSN GURNARD Data with Satellite TIR DATA 12

   4.1 Introduction 12

   4.2 Preparing the Two Data Sets 15

   4.3 Registration of Satellite and Submarine Data 15

   4.4 Correlation Functions 20

5. Correlation of Simultaneous Airborne TIR Data with Under-Ice Data by HMS SOVEREIGN 22

   5.1 Introduction 22

   5.2 Data Analysis 22

      5.2.1 Under-Ice Data 22

      5.2.2 Airborne TIR Data 25

   5.3 Correlation of Under-Ice Roughness with Skewness of Surface Temperature Distribution 27

6. Discussion of the Data 33

7. Conclusions 36

8. References 38

9. Acknowledgement 40

Appendices

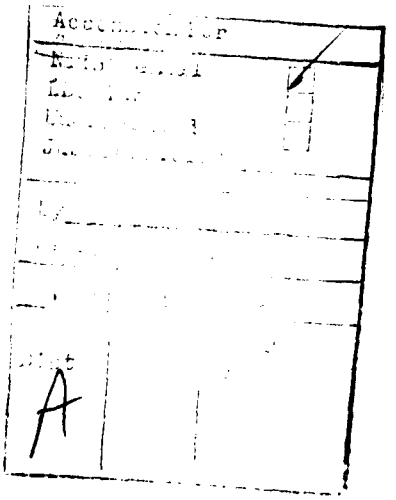

1. Background

Since 1973 the author has been examining the statistical properties of Arctic sea ice thermal infrared (TIR) temperature measurements obtained with VHRR satellites (LeSchack, 1974; 1975; 1976a). The thrust of that research was to determine whether it is feasible to objectively (i.e., numerically) identify different sea ice types and develop a system for automated mapping of sea ice. At a conference where the results of the above studies, along with those of submarine under-ice analyses were presented (LeSchack, 1976b), Buck (1975) made the observation that it would be valuable to his under-ice acoustic work if some correlation could be found between the satellite and submarine data sets, both recorded in the eastern Beaufort Sea. Although the idea of making a large area correlation between submarine and airborne or satellite data of sea ice was not new (see for example, Barnett, 1966), this was the first time that two data sets usable for this task became available. Accordingly, with both the availability of the necessary data and the impetus provided by a concrete use for any correlations developed, work was begun in 1976 to investigate the relationship between satellite and submarine under-ice roughness data.

2. Under-Ice Roughness

The variable that we wish to ultimately predict is under ice roughness, since this variable strongly influences acoustic propagation beneath the ice. Several mathematical definitions of under ice roughness can be formulated; however, only two forms appear significant to our problem. These are the root-mean-square (RMS) under-ice depth and the standard deviation, σ, of the under-ice depth, respectively defined as:

$$RMS = \left[\frac{\sum_{i=1}^{N} \left(x_i^2 \right)}{N} \right]^{1/2} \tag{1}$$

and

$$\sigma = \left[\frac{\sum_{i=1}^{N} \left(x_i - \bar{x}^2 \right)}{N} \right]^{1/2} \tag{2}$$

where

x = value of under ice depth in m (depth of ice from water line)
N = number of depth values along a profile

At the outset of this work, RMS under ice roughness was the parameter of choice. This was because not only is it a measure of roughness, but it appears to be a good indicator of overall ice deformation for a given ice surface area, since any significant departure from the undeformed equilibrium ice depth over the Arctic Ocean (about 3 m) can occur only through building ice ridges and keels or opening of leads and polynyas.

As the work progressed, however, the standard deviation, σ, of the ice depth was suggested by Buck (1977) as being more meaningful to the acoustic attenuation problem than was the RMS ice depth; therefore, in subsequent work, σ was used. As we shall see, there is a close correlation between these measures of under ice roughness, as well as the "ice roughness factor" suggested by Buck (1979).

The under-ice data used for the early portion of this work were collected on three submarine cruises (Figure 1) and were discussed in detail in LeSchack and Chang (1977). The SSN SARGO collected data during February 1960, and two cruises were made by the SSN SEADRAGON during the summers of 1960 and 1962. Selected RMS ice depth values from each cruise are plotted on Figure 1. From this plot, a general trend of increasing RMS ice depth from West to East appears, with maximum values occurring along the Canadian Archipelago (Figure 2). Comparison of these data distributions with the distributions of "ridging intensity" values of Hibler *et al* (1974) in the Western Arctic Basin shows that the RMS ice depth values can be well delineated by the three ice ridging provinces which they call Beaufort-Chukchi, West Central Arctic Basin, and Archipelago. Since the data of Hibler *et al* (1974) were recorded a decade after the submarine data were gathered, a stable pattern of ice deformation provinces over time is suggested. Additional under-ice data recorded by the SSN GURNARD in 1976 (to be discussed later) and the statistical analysis of the 1960-1962 data (LeSchack and Chang 1977) are also consistent with the suggested stable under-ice roughness pattern of the Arctic permanent pack.

As mentioned above, preliminary comparisons between standard deviation, mean ice depth, RMS ice depth and "ice roughness factor" have been made. Figure 3 shows the interelationship between the mean ice depth, the RMS ice depth and the standard deviation for the data recorded by the SSN GURNARD. In Figure 4 the standard deviations of ice depths recorded on the 1960 cruise of the SSN SARGO have been compared with the "ice roughness factor" of Buck (1979). This factor is defined as the product of the number of keels equal or greater than 2 m per 50 km and the square of the mean ice depth for the same 50 km ice profile section. This factor is similar to the "ice ridging intensity" of Hibler *et al* (1974).

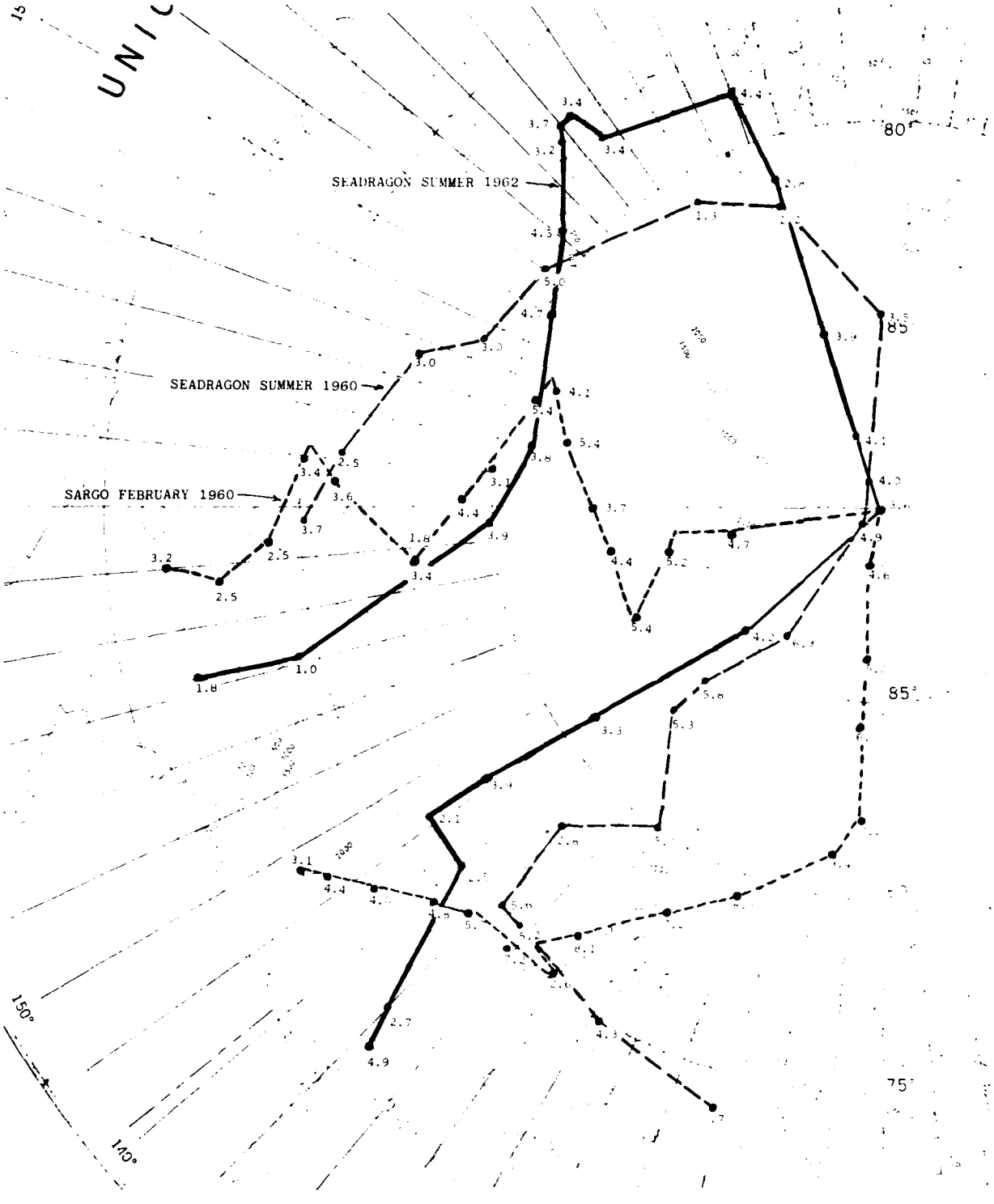

FIGURE 1: Cruise tracks of the SSN SARGO in February 1960 and the SSN SEADRAGON in the summers of 1960 and 1962. A sampling of RMS ice depths (m) along each track is included. Each data point was derived from a segment of under-ice profile approximately 8 nautical miles in length. (Modified from Lyon, 1963)

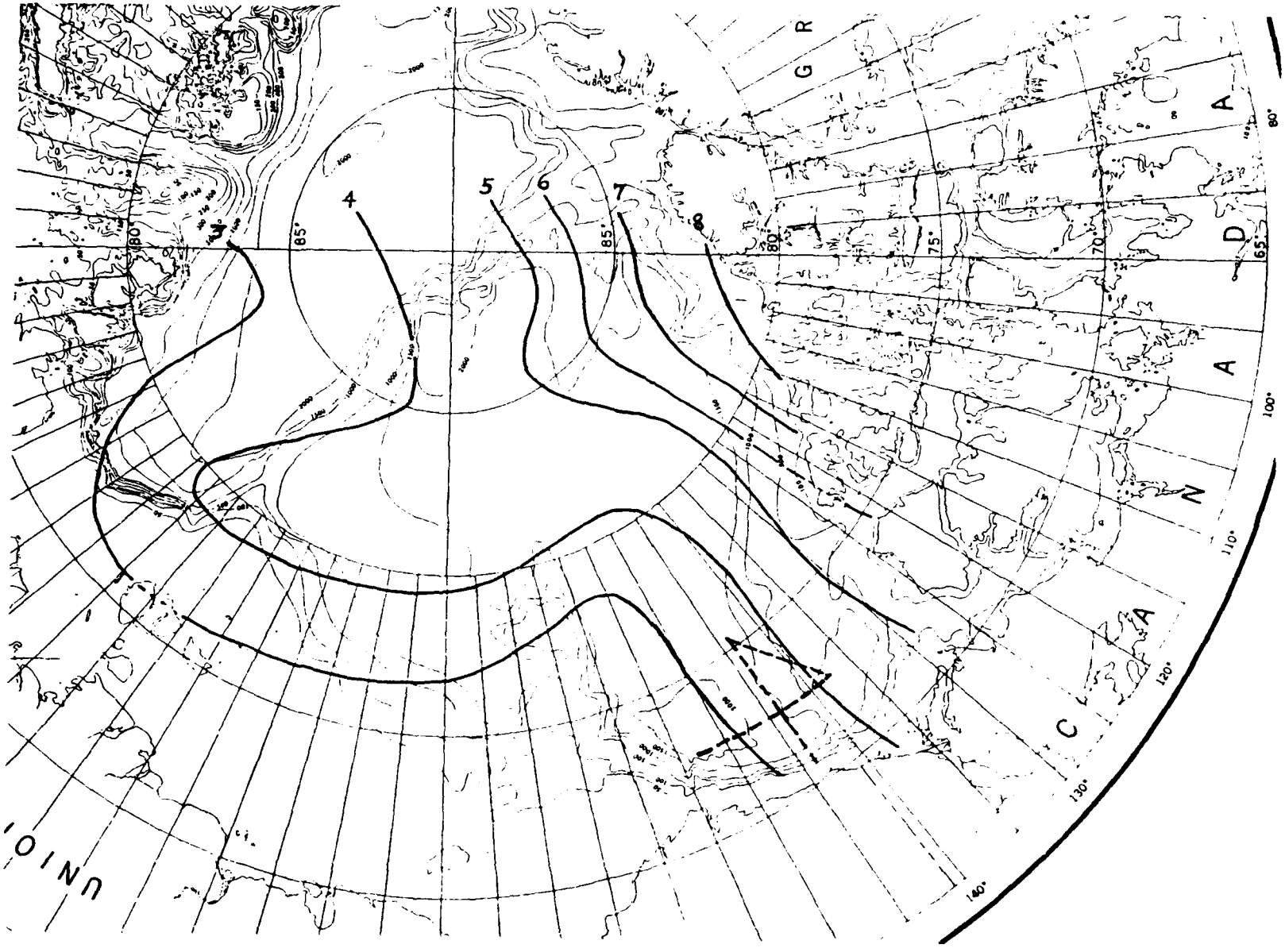

FIGURE 2: A contour map of mean RMS ice depths (m) based on the 1960-62 under-ice data shown in Figure 1. The 1976 track of the SSN GURNARD is shown in dashed lines. The overall mean RMS ice depth for this cruise was 4.3 m. Considering the accuracy of our contours, the 1976 data appears to fall into the same ice province as does the 1960-62 data.

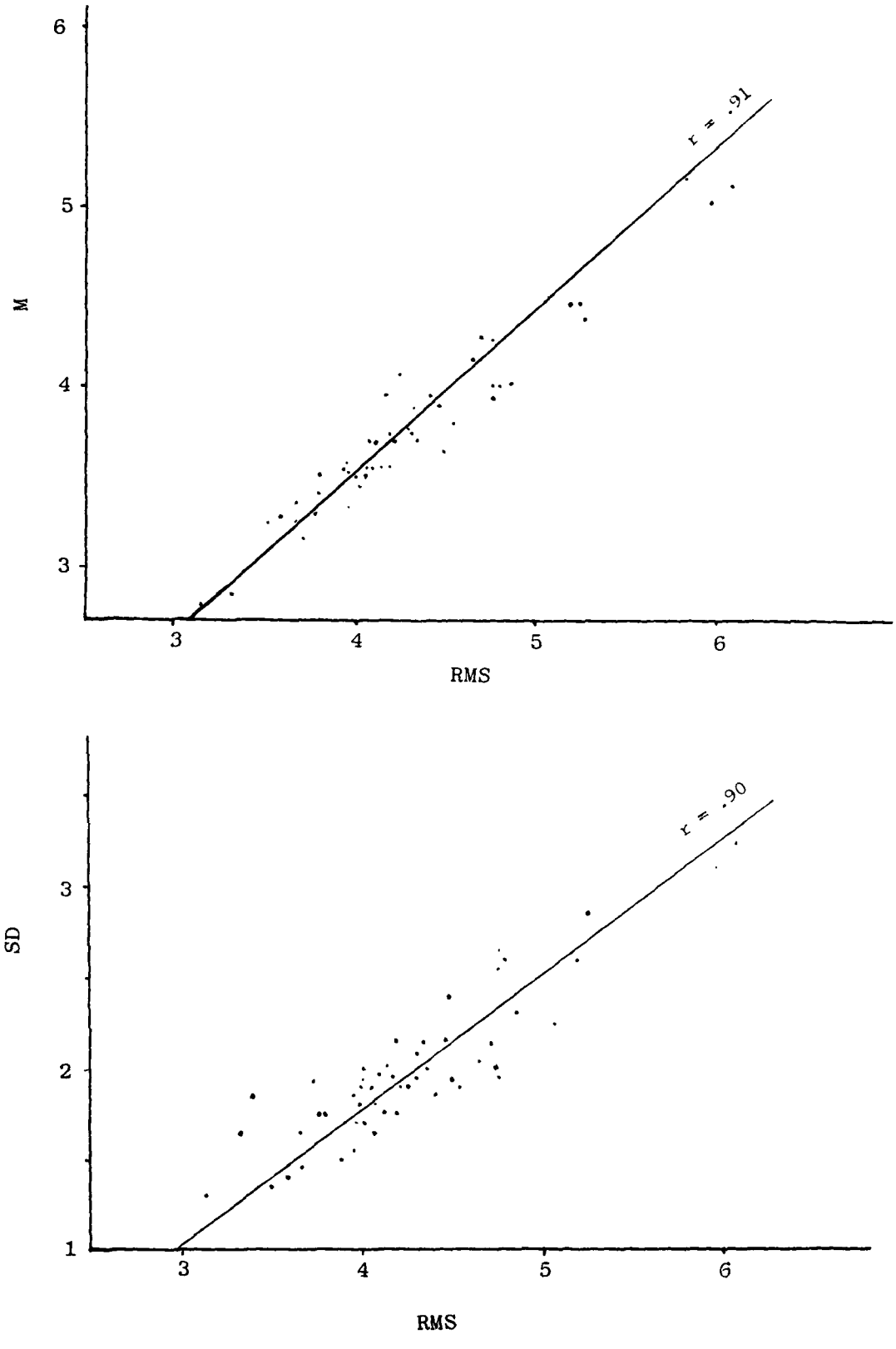

FIGURE 3: Good correlations can be seen between mean ice depth and RMS ice depth (above) and standard deviation and RMS ice depth (below) for the SSN GURNARD data. Each data point represents a 10 N-mile average.

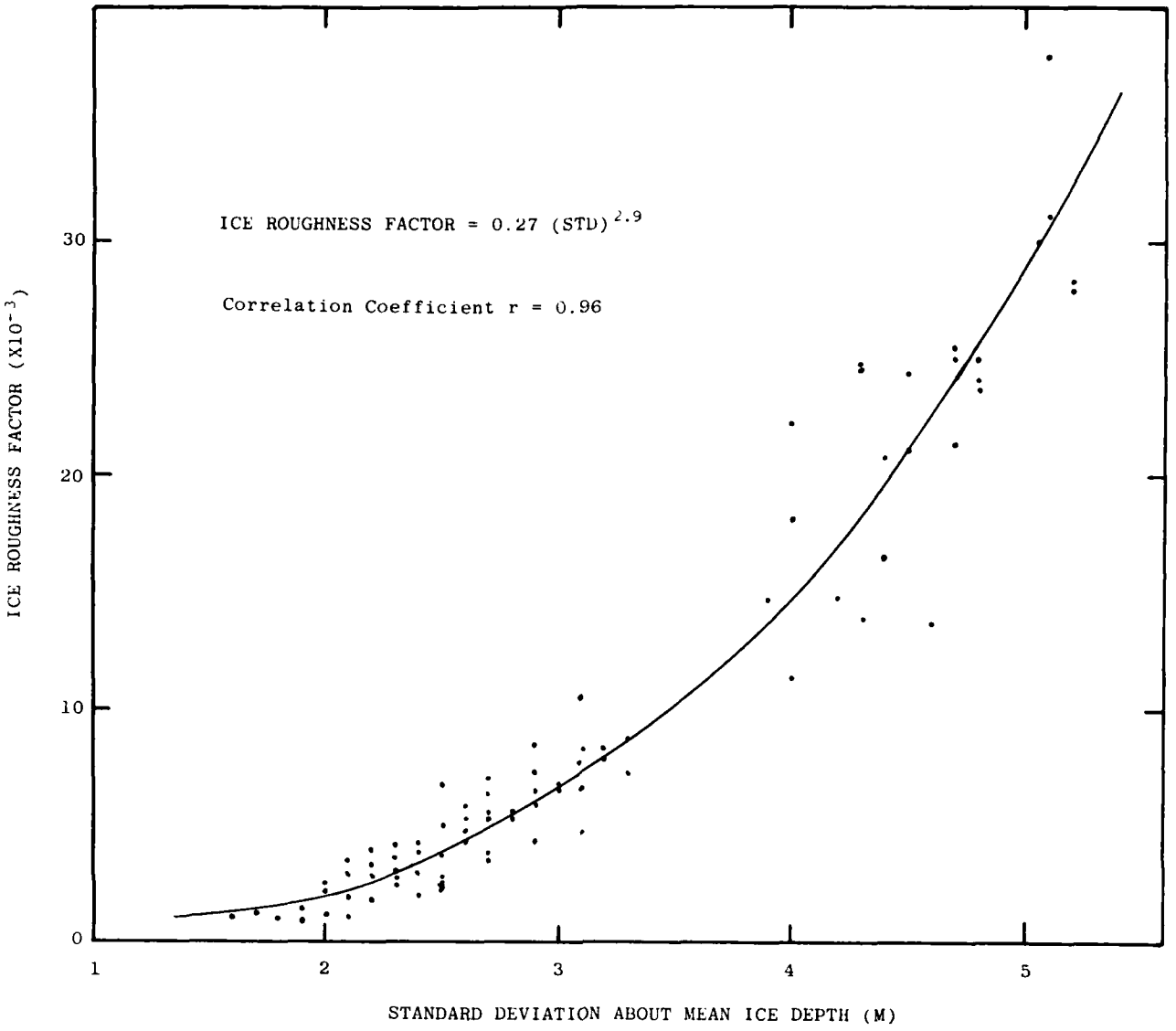

FIGURE 4: Plot of Ice Roughness Factor (see text) *vs* standard deviation about mean ice depth. Each data point is derived from a 50-km profile section from the 1960 winter cruise of the SSN SARGO.

As can be seen from both Figures 3 and 4, there appears to be a close relationship between all measures of under ice roughness that have been used by various researchers. As a result, the three following examples of correlations of TIR data with under-ice roughness have been presented as they were originally computed, the first two with RMS values, and the last with values of standard deviation, since the object of the work to date has only been to establish the existence of a functional relationship between TIR and under-ice roughness data.

3. Preliminary Correlation of RMS Ice Depth with Satellite TIR Temperature Data

Evidence from previous research (LeSchack, 1974, 1975, 1976a), revealed that when a statistically sufficient number of surface temperature measurements were made of the undeformed multi-year ice surface in the Arctic, using airborne or satellite TIR scanners, the measurements would fall into a normal or Gaussian distribution. As the ice deformed, the surface temperature distribution skewed toward the side of the curve corresponding to the lower temperatures. The temperature distribution appeared to skew more with the greater amounts of deformation.

The physical basis for this relationship, to be discussed in greater detail in a forthcoming report, appears to relate to surface ice roughness only indirectly. The reasons for an increased number of colder infrared temperature measurements with increased ice deformation appear to relate to how the TIR scanner perceives the roughened surface, rather than to any direct sensing of lessened heat flow due to thicker ice in deformed areas. From an analysis of the sea ice surface, the following factors seem to be of greatest importance. With increasing ice deformation:

(1) there is an overall increase in snow catchment, thus reducing the surface temperature directly and because snow's emissivity is less than that of sea ice, reducing also the TIR scanner's perception of the surface temperature.

(2) there is an increase of shadowing of the sun's radiation during daylight hours, relative to an undeformed surface. These shadow areas will naturally be cooler than irradiated areas.

(3) there is an increase in aerodynamic surface roughness, This effect, depending on conditions, may result in either slightly increased or decreased surface temperature.

LeSchack (1974, 1975) have shown by statistical analysis of radiant temperature data distributions for given areas of

the ice surface, as obtained by the NOAA VHRR satellite, that an objective identification can be made of the various surface types, i.e., first-year ice, multi-year ice, water, landfast ice, land, and clouds. LeSchack (1975) notes, for example, that an area of all multi-year ice produces a normal distribution of temperature data points with a mean value close to that predicted by the model of Maykut and Untersteiner (1971), with a skewness of zero and a kurtosis (peakedness) of about 3.[1] If increasing areas of warmer first-year ice are included in the area surveyed, the temeprature distribution skews positively. If the area includes colder clouds, the distribution skews strongly in the negative direction (<-0.20). If there is a lot of ridging of the multi-year ice, the temperature appears colder than the mean multi-year ice, thus producing a modest negative skewness. Therefore, if by the selection techniques discussed in LeSchack (1975) a large expanse of ice surface can be identified without cloud cover, it should be possible to predict the general extent of surface ridging by analyzing the skewness of the temperature distribution.

Figure 5 is an IR image recorded over the Western Arctic Basin on 17 April 1974. The area enclosed in the square (approximately 500 x 500 N. miles) includes the Beaufort-Chukchi, West Central Arctic Basin, and Archipelago regions outlined by Hibler *et al* (1974). The area enclosed on the image has been computer processed so that individual arrays of radiant temperature data can be examined statistically. Each array consists of a 32 x 32 array of 1-km imagery resolution elements. As mentioned above, it has been possible to characterize this entire area by the mean temperature, the skewness and the kurtosis of each 32 x 32 km array. If the skewness matrix (Figure 6) for the area shown on the imagery in Figure 5 is now examined, it can be seen that a transect can be picked that extends more than 500 miles in length, through a cloud-free section of ice. This transect crosses all three of the ridging provinces discussed by Hibler *et al* (1974) and furthermore, comes close to paralleling the track made by the SSN SARGO cruising beneath the ice in February 1960.

Figure 7 shows a section of the SSN SARGO track that nearly coincides with the transect shown in Figure 6. At several random locations, RMS ice depths for 8-mile segments have been computed from the under-ice profiles recorded by the submarine's upward-looking sonar. The transect shown in Figure 6 has been divided in approximately equal area segments that correspond closely to the locations for five of the RMS ice depth values plotted on Figure 7 (the value associated with the shear zone segment, i.e., the large shaded area on Figure 6, has not been used since this area contains considerable first-year ice with

[1]For an explanation of these terms see Appendix A.

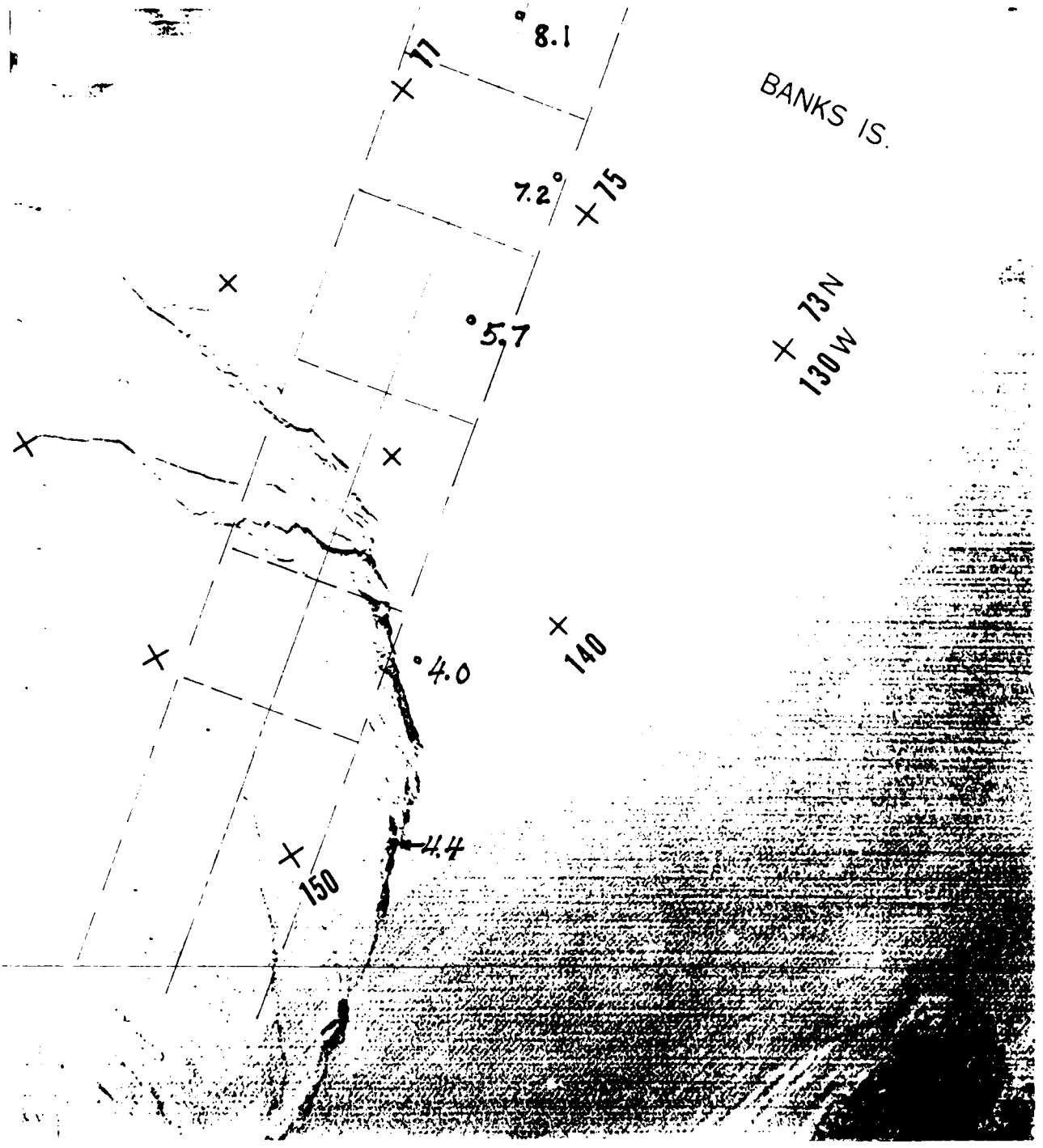

FIGURE 5: NOAA VHRR infrared satellite imagery of the Western Arctic Basin recorded on 17 April 1974. This area has been numerically analyzed and values of the skewness of the surface temperatures are presented in Figure 6. All three of the ridging intensity provinces discussed by Hibler et al. (1974) are included within the area, which is approximately 500 x 500 n. miles. A NEE-SWW transect has been chosen for comparison of skewness with some RMS ice depth values (bold-face numbers, in meters) derived from the February 1960 under-ice profile data recorded by the SSN SARGO shown in Figure 7.

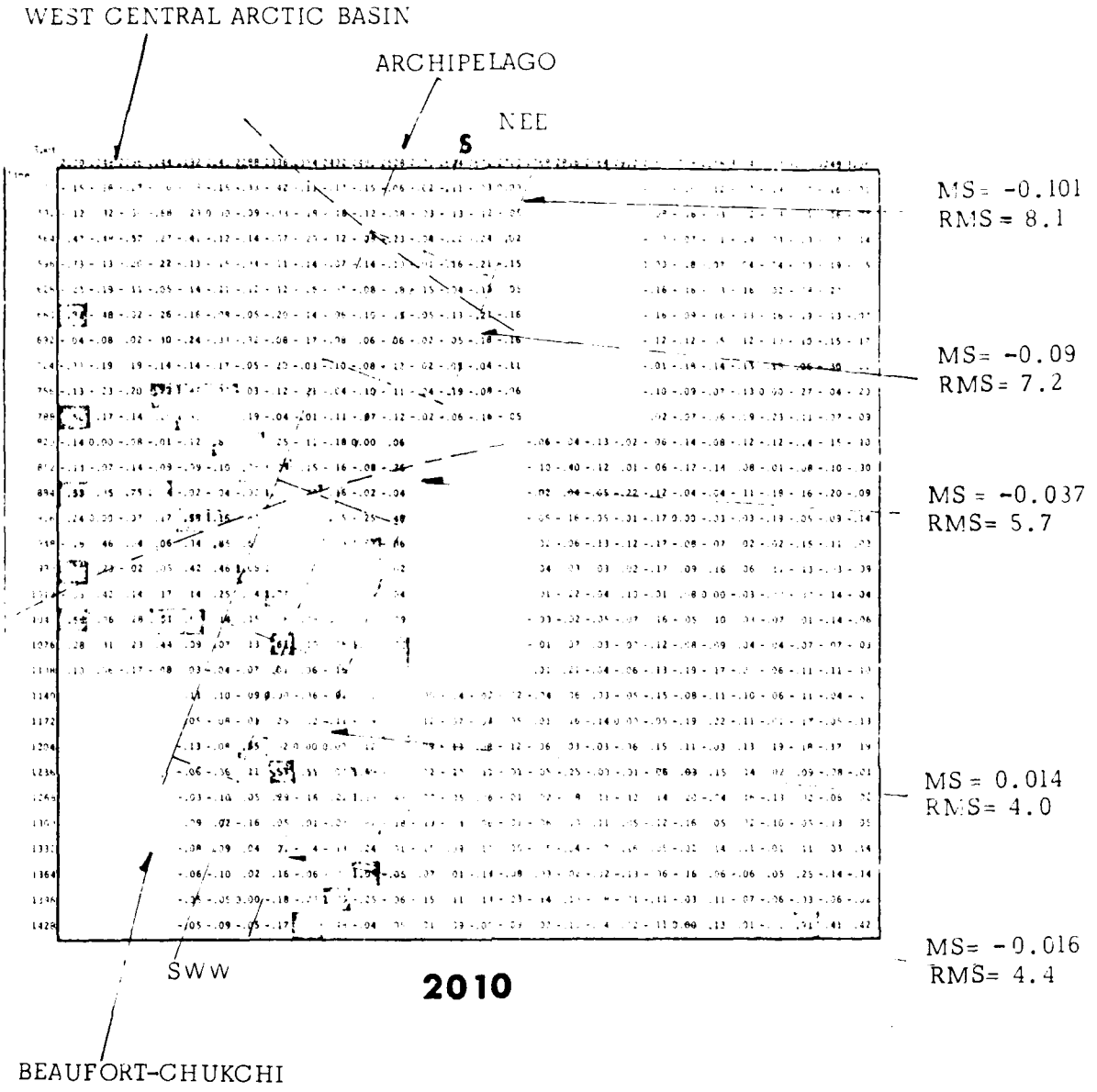

FIGURE 6: A matrix of the skewness of the ice temperature distribution for the imagery shown in Figure 5. Each skewness value was derived from a 32 x 32 km array of temperature data. The width and sections of the transect were arbitrarily chosen such that an adequate sample of skewness data could be compared with an RMS ice depth value derived from a region of close proximity. The mean skewness (MS) and RMS ice depth (RMS, in meters) are tabulated for each section at right. Banks Island is at upper righthand corner. Ridging provinces are delineated. The shaded areas have a skewness $\geq$ 0.50, which implies much first-year ice.

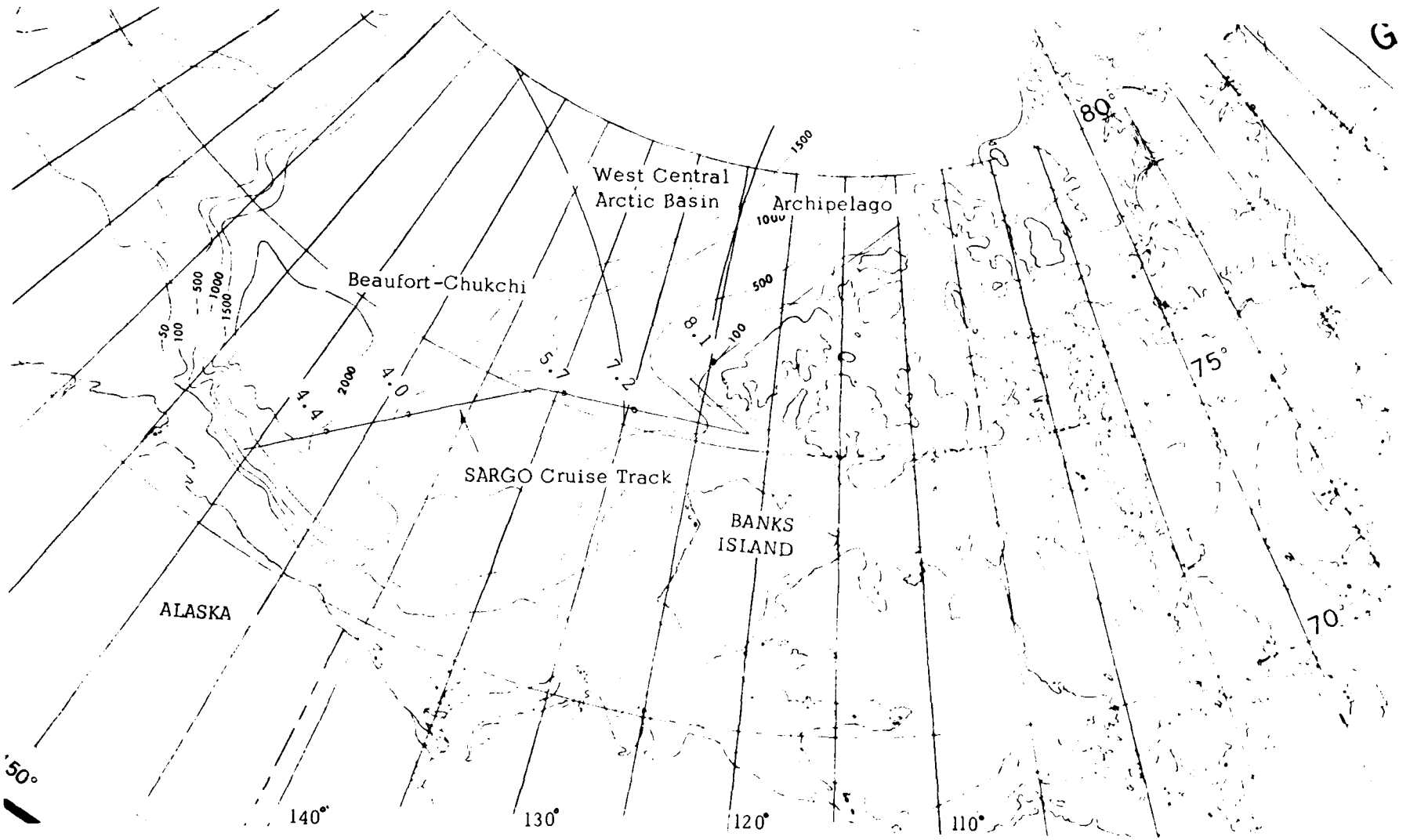

FIGURE 7: Superimposed along the February 1960 cruise track of the SSN SARGO are values of RMS ice depth (m). The general boundaries of the three "ridging intensity" provinces described by Hibler *et al* (1974) are indicated.

resulting high positive skewness values). When the data pairs (i.e., the skewness and the RMS values) for each area are plotted, a clear negative linear relationship emerges (Figure 8). For this to be a meaningful correlation, we must assume that the ice provinces in 1960 were essentially the same as they were in 1974. However, the work by Hibler *et al* (1974), the statistical analysis of LeSchack and Chang (1977), and the consistency of the SSN GURNARD data of 1976 with the 1960-62 data shown in Figure 2 all suggest that the type of ice roughness stability as expressed by the statistical parameters used above is possible.

4. Correlating SSN GURNARD Data with Satellite TIR Data

4.1 Introduction

The correlation shown in Section 3 above is startling. However, since only five data sets were available for the regression line shown in Figure 8, and because of all the assumptions as to ice province stability that are necessary before this Figure is meaningful, an attempt was made to try this correlation again with a new set of data.

In April 1976, the SSN GURNARD gathered under-ice roughness data along three straight-line tracks, each about 200 N. miles long, in the vicinity of the AIDJEX Project. The cruise tracks are shown in Figure 2. A cloud-free VHRR IR image was obtained for this area of the Beaufort Sea for 8 March 1976, about a month earlier than the cruise. The cruise tracks were laid out on the rectified imagery (Figure 9) and 16 x 16 km squares of TIR data (each containing 256 pixcels) along these cruise tracks were then selected for analysis. A total of 58 16 x 16 km (10 x 10 N. mile) data squares were found to lay along the cruise tracks. A statistical analysis of the temperature distribution of each of these squares was then made. By photo-interpretive techniques a determination was made as to which of the 58 blocks were all multi-year ice. Some 22 blocks were chosen.[1] At this stage of the research it appears necessary to use only multi-year ice for the correlation analysis; mixtures with first-year ice have distorted skewness patterns that are not as easy to correlate with under-ice data as are the pure multi-year ice distributions.

Although at first glance, the requirement to choose only multi-year ice distributions for analysis purposes may seem limiting in the context of conducting a large-scale survey, in fact, the selection process appears easy to do by computer, an important criterion for any operational use of this prediction technique. Figure 10 is a plot of TIR temperature skewness *vs* kurtosis for the 58 16 x 16 km data blocks chosen. It is signifi-

[1] Appendix B contains a tabulation of these data.

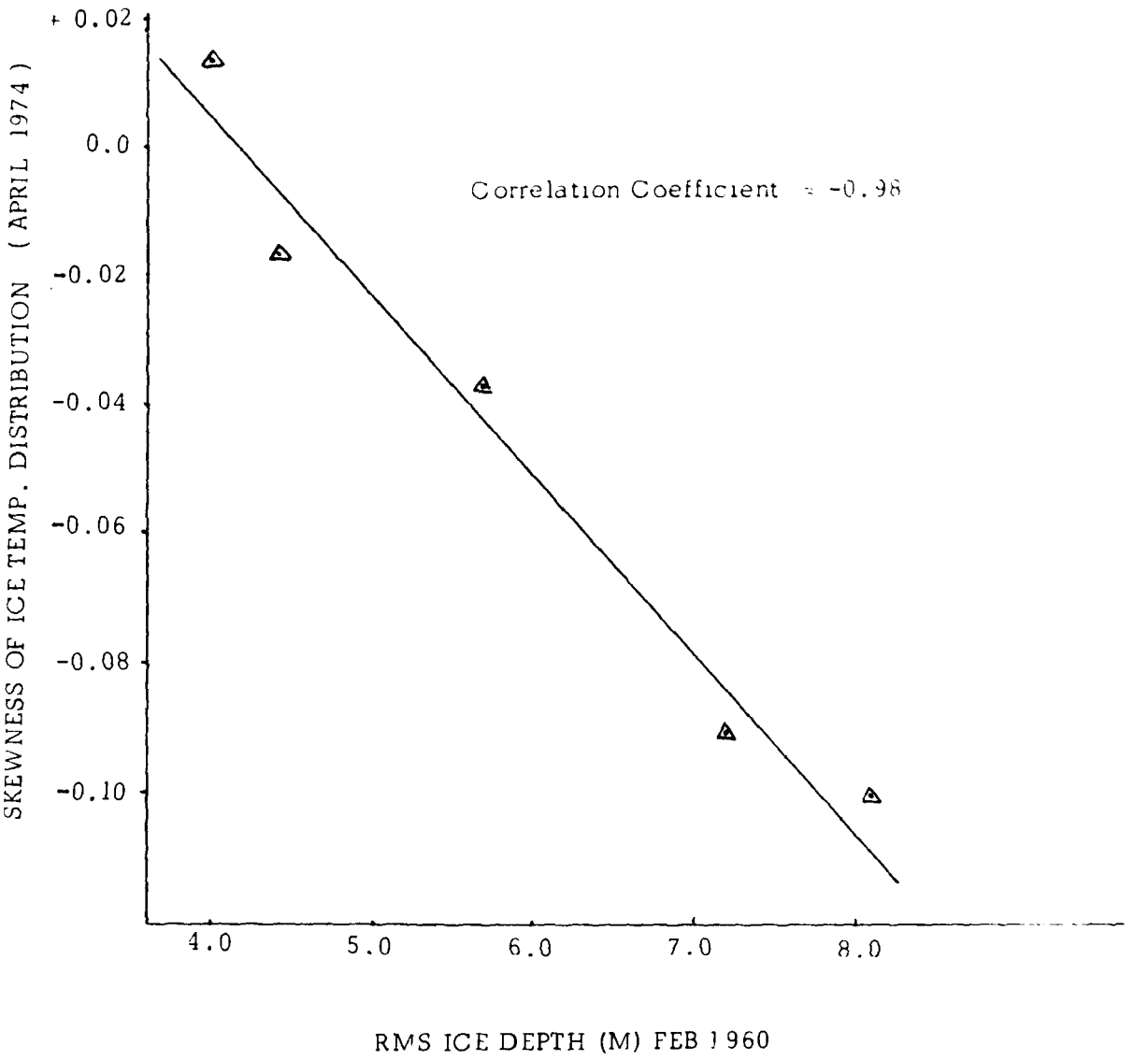

FIGURE 8: **A strong negative correlation between RMS ice depth and skewness of the ice surface temperature as measured by NOAA VHRR satellites is observed for the few locations where these data are available.**

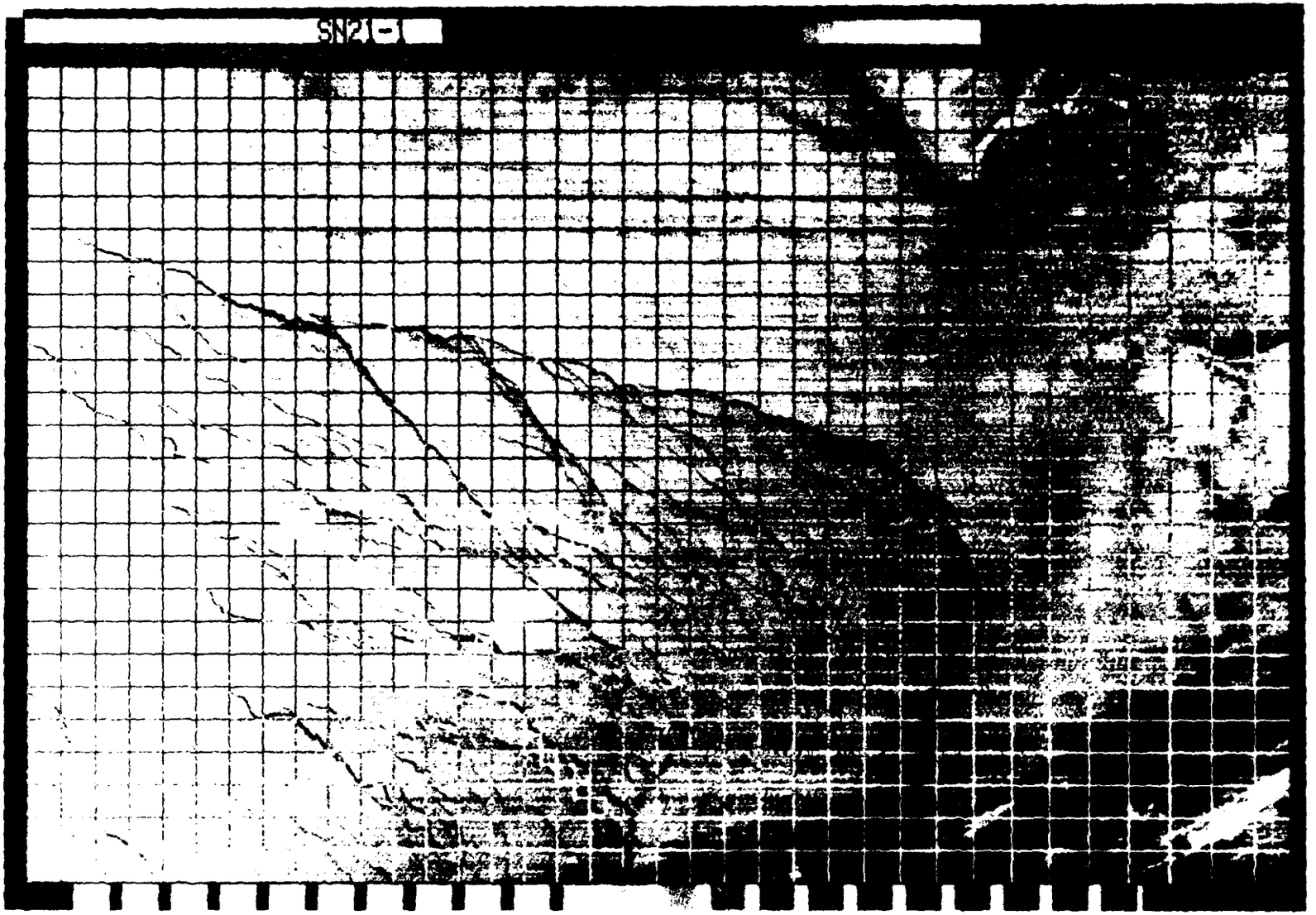

FIGURE 9: A rectified IR image of the eastern Beaufort Sea recorded by NOAA VHRR satellite on 8 March 1976. Sachs Harbour, Banks Island is in upper right-hand portion of image. Large grid divides image into 32 x 32 km squares (made of 1024 resolution elements). The smaller squares (16 x 16 km) in the lower left-hand portion of the image lie along the cruise track of the [illegible].

cant that essentially all of the data points identified by photo-interpretation as being pure multi-year ice are clustered together, whereas data representing a variety of mixtures of multi-year ice and first-year ice are scattered about the plot in no order as yet discernible. This appears significant since, as suggested by Figure 10, an algorithm can be easily constructed to select, with high probability, all the pure multi-year ice data in a given population.

4.2 Preparing the Two Data Sets

The most obvious criticism of the correlation presented in Section 3 is that the satellite data were recorded 14 years after the submarine data. In the case of the SSN GURNARD data, however, satellite data of the area were available for the previous month. From past experience, it is reasonable to assume that during the March-April period there will be little physical change in the ice, although as can be seen from Figure 11 a westerly drift might be expected. Accordingly, a comparison of satellite and submarine data taken only a month apart can, with adjustment for ice movement, be considered to be made between simultaneously recorded data.

4.3 Registration of Satellite and Submarine Data

In the data compared in Section 3, a broad ice surface (some 160 km on a side) was analyzed to obtain the five individual skewness values used for the correlation shown in Figure 8. Each of the five individual skewness values represented ice conditions for a whole province rather than a small area, and as a result, exact registration of the satellite data and the under-ice data with which it was compared appeared unnecessary. In the case of the SSN GURNARD data, however, a 1:1 correlation with the satellite data, broken up into 16 x 16 km elements, is being attempted. Accordingly, the three legs of the cruise have been divided into adjacent 16 km (10 N. mile) profile segments (Figure 12). The mean RMS ice depth for each segment was computed and tabulated with the 22 temperature skewness values determined to be representative of pure multi-year ice (Table 1). The skewness data have been plotted in the geographical position along the submarine tracks corresponding to a direct overlay of data sets; i.e., the 16 x 16 km satellite data blocks have nominally the same coordinate position as the submarine data beneath them, notwithstanding the fact that some ice movement is anticipated.

Examination of the ice drift records for this period shows a movement of 10-20 N. miles in the western quadrant (Thorndike and Cheung, 1977). Accordingly, it was felt that some shifting of the data sets might be necessary to effect data registration. Figure 12 illustrates the data matrix configuration. If the satellite data matrix is moved north one block (16 km) (and we assume no horizontal deformation of the ice sur-

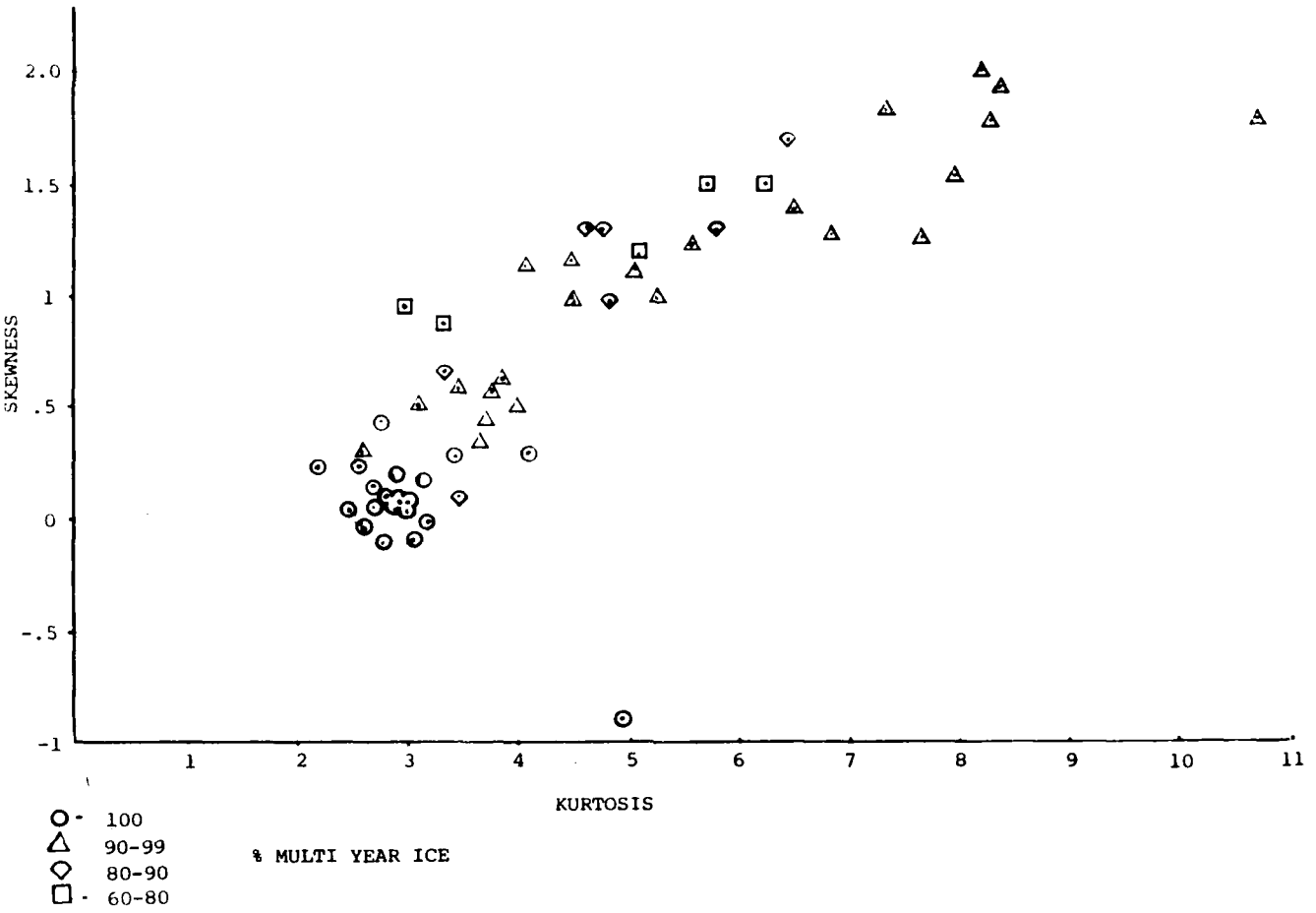

FIGURE 10: A plot of skewness *vs* kurtosis of temperature distributions derived from the 58 16 x 16 km data squares along the track of the SSN GURNARD shown in Figure 9. (See Appendix B for data). Multi-year/first year ice mixtures have been determined by photo-interpretation of the VHRR image. Note that all of the pure multi-year ice data cluster at the bottom of the plot

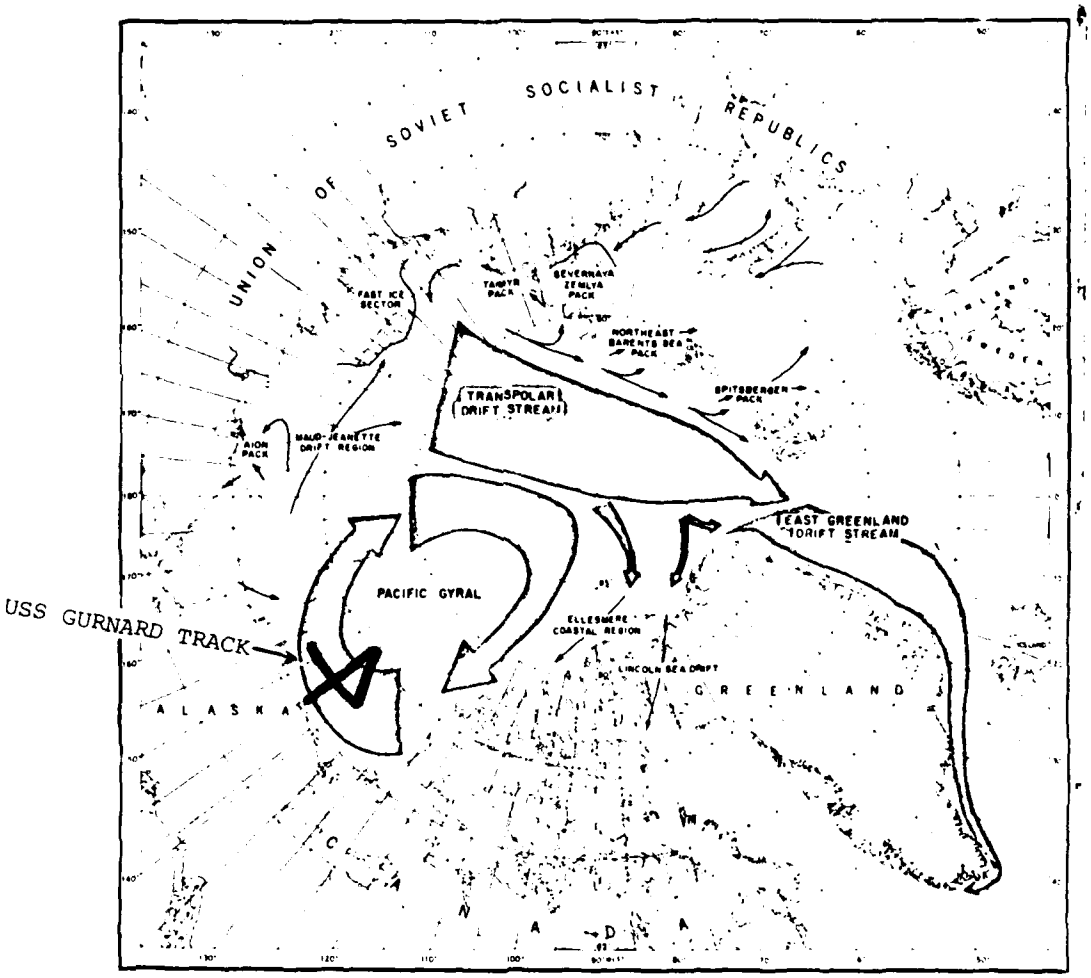

FIGURE 11: The major drifts of polar ice (after Dunbar and Wittman, 1963). Note that the SSN GURNARD track falls within the westerly-moving ice.

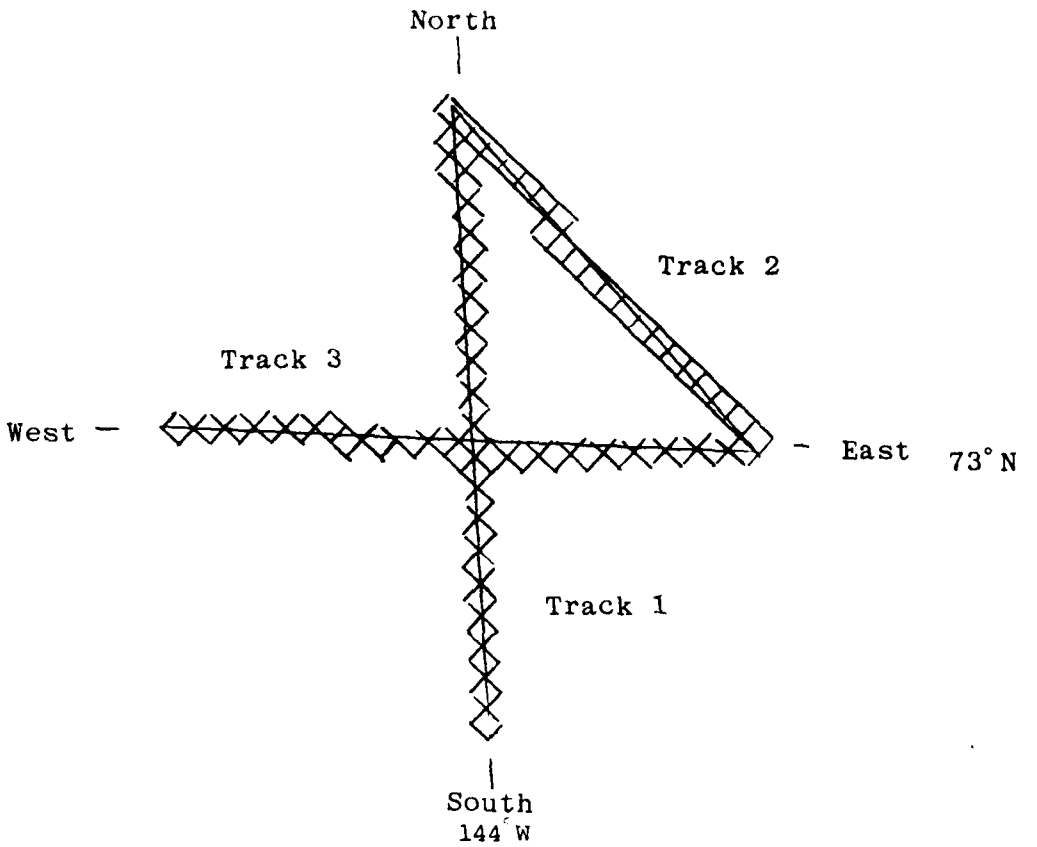

SSN GURNARD Track

16 x 16 km squares of VHRR TIR data

FIGURE 12: A nominal overlay of satellite VHRR data on the RMS under-ice data. Each track was appropriately divided into sections of sufficient length to match the corresponding VHRR data blocks. The two data matrices can be shifted until the best registration is obtained.

Table 1: Comparison of Under Ice Roughness with Nominally Overlain VHRR Skewness Data

Track 1																						
RMS	S	5.82	6.07	4.78	5.23	4.12	4.18	4.40	4.86	4.30	3.42	4.47	4.19	3.33	3.67	3.98	4.00	4.17	3.97	3.80	4.07	
SKEW.							0.18	0.05			0.05	0.08			0.33	0.14	0.12	0.05		0.00		N
Track 2																						
RMS	NW	3.77	4.01	3.95	4.34	4.09	4.76	4.22	4.12	4.25	4.76	4.07	3.88	4.02	3.66	3.78	3.96	3.52	3.50	4.47	5.25	
SKEW.						0.24	0.44						0.00		0.05	0.12		-0.11				SE
Track 3																						
RMS	E	4.33	4.46	4.48	4.06	4.37	4.02	3.73	4.23	3.59	4.32	4.71	4.54	3.15	4.74	4.50	4.76	5.06	5.19	5.96	4.66	3.91	4.58	4.82
SKEW.						0.26	-0.29			0.09							-0.08		-0.91	-0.04	-0.17			W

Note: The above is the no-shift position, hence for Track 1 there will be 9 data pairs, i.e., 4.18, 0.18; 4.40, 0.05, etc. For Track 2, 6 data pairs, i.e., 4.09, 0.24; 4.76, 0.44 etc. For Track 3, 7 data pairs, i.e., 4.37, 0.26; 4.02, -0.29 etc. This will make a total of 22 data pairs. For a skewness matrix data shift of, for example, 1 block north, the skewness matrix for Track 1 will move 1 block north generating 9 data pairs as follows: 4.40, 0.18; 4.86, 0.05 etc. The skewness matrix for Track 2 will move 1 block to the northwest generating 6 data pairs as follows: 4.34, 0.24; 4.09, 0.44 etc. The skewness matrix for Track 3 will not shift, generating 7 data pairs as before, i.e., 4.37, 0.26; 4.02, -0.29 etc. In all, 9 sets of 22 data pairs (and then 20, when 2 points were discarded) were generated from the above 3-Track matrices. The correlations are shown in Table 2.

face), the result will be a 1 block north shift along track 1, approximately a 1 block northwest shift along track 2, and no shift along track 3. Similarly, shifting of data along the three tracks resulting from moving the satellite data matrix to the NE, E, SE, S, SW, W, and NW can likewise be accomplished, and by referring to Table 1, a different set of data pairs for each shift can be derived for computing correlation functions. Since Thorndike and Cheung (1977) indicated movement of only 10-20 N. miles, a maximum matrix shift of only one data block (10 N. miles) was considered necessary for determining data set registration.

4.4 Correlation Functions

Since the major thrust of the work with the SSN GURNARD data was to verify whether the correlation presented in Figure 8 is real, the next step is to attempt to correlate the April 1976 under-ice data with the March 1976 satellite data of the same area. Using the two data matrices presented in Table 1 and allowing either no ice shift or a 10-N. mile shift along the eight compass points, 9 different sets of 22 data pairs can be generated. Although in the case of Figure 8 the small number of data points and their obvious linear relationship makes it reasonable to attempt only a linear fit to the data, a linear, parabolic, exponential, logarithmic and power fit were attempted with the SSN GURNARD data. The parabolic fit in all cases provided the best correlation, with the linear fit next best. The 9 sets of correlation results are presented in Table 2, first using all 22 data pairs and then eliminating two data pairs because their skewness values appeared too high to be truly representative of pure multi-year ice (the removal of these two pairs is based solely on an intuitive feel for the data, but as will be seen shortly, appears reasonable).

Examination of the correlations in Table 2 indicates that only when the satellite data are shifted SW, W or NW, relative to the submarine data are there any significant correlations. In Figure 13, these correlations are shown graphically when the parabolic correlation coefficients, r, for the 20 data pairs are plotted around the points of the compass. Only does movement in the western quadrant appear statistically meaningful while movement in the quadrants away from the west produces monotonically decreasing correlation. This is consistent with the westerly ice movement in the March-April 1976 period, i.e., the satellite data matrix had to be shifted to the west to come into register with the submarine data. This strongly suggests that not only is there a good correlation between the satellite TIR data and the submarine under-ice roughness data but that the correlation is meaningful down to resolution elements of 16 km (10 N. mile) on a side.

TABLE 2: Linear and Parabolic Correlations of the Satellite Data Shifted 10 N. Miles with Respect to the Submarine Data

SHIFT	22 Data Points Linear (r)	Parabolic (r)	20 Data Points Linear (r)	Parabolic (r)
None	-.28	.30	-.34	.36
S	-.40	.41	-.38	.39
SW	-.55	.75	-.67	.89
W	-.65	.81	-.66	.88
NW	-.64	.84	-.65	.89
N	-.41	.42	-.38	.40
NE	-.18	.20	-.23	.30
E	-.23	.26	-.19	.22
SE	-.28	.33	-.23	.28

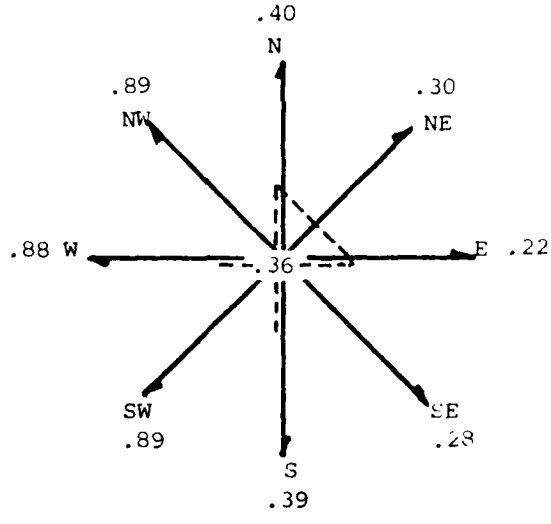

FIGURE 13: A strong correlation is observed in the western quadrant when the correlation coefficient (r) is plotted around the points of the compass (See Table 2).

It is instructive to examine a plot of the skewness vs RMS data for one of the shifts that produces a good correlation. Figure 14 is a plot of the SW shifted data. The two points that have been eliminated from one of the sets of correlations have been indicated on the plot. They have been eliminated both on the grounds that they do not seem to cluster with the remaining data and that a skewness of greater than +0.3 probably indicates warm clouds over the ice or first-year ice mixed with the multi-year ice, either of which adversely affects the relationship of skewness to ice deformation. The remaining data points appear generally to be scattered equally around the curve fit to the data.

5. Correlation of Simultaneous Airborne TIR Data with Under-Ice Data by HMS SOVEREIGN

5.1 Introduction

A third study was then conducted that shows, perhaps more graphically than the others, the correlation of under-ice data recorded by the British nuclear submarine HMS SOVEREIGN between 18-21 October 1976 with airborne TIR data recorded during the same period over the submarine track by a Canadian Forces Argus aircraft. In many ways, this example is better than the previous two. The airborne TIR data are recorded in the form of imagery on a scale large enough to see the individual features of the ice surface. Every attempt was made to cover the exact track of the submarine within hours of its passing beneath the ice.

Figure 15 shows the submarine track. The data discussed in this example were collected along Segment AB. Wadhams (1978) divided Segment AB into 10 sections, each approximately 97 km in length. They are numbered as in Figure 15. The airborne TIR data used in this correlation were recorded from an altitude of 4000 ft (1200 m) between 1910 hrs and 2109 hrs Z on 19 October 1976 along Segment AB. The exercise was referred to as "Brisk Laser #1" by the Canadian Defense Research Establishment.

5.2 Data Analysis

5.2.1 Under-Ice Data

As in the previous Beaufort Sea examples cited, the object of this work is to derive an under-ice roughness parameter from the profile data, and to correlate it with a parameter easily derived from the airborne TIR data that physically relates to the topside roughness of the ice. Although in the previous examples the RMS ice depth was used as the under-ice roughness parameter, recent work by Buck (1979) indicates standard deviation (σ) from the mean under-ice depth is more meaningful for Arctic acoustics. Therefore, σ will be the under-ice roughness parameter used in this example.

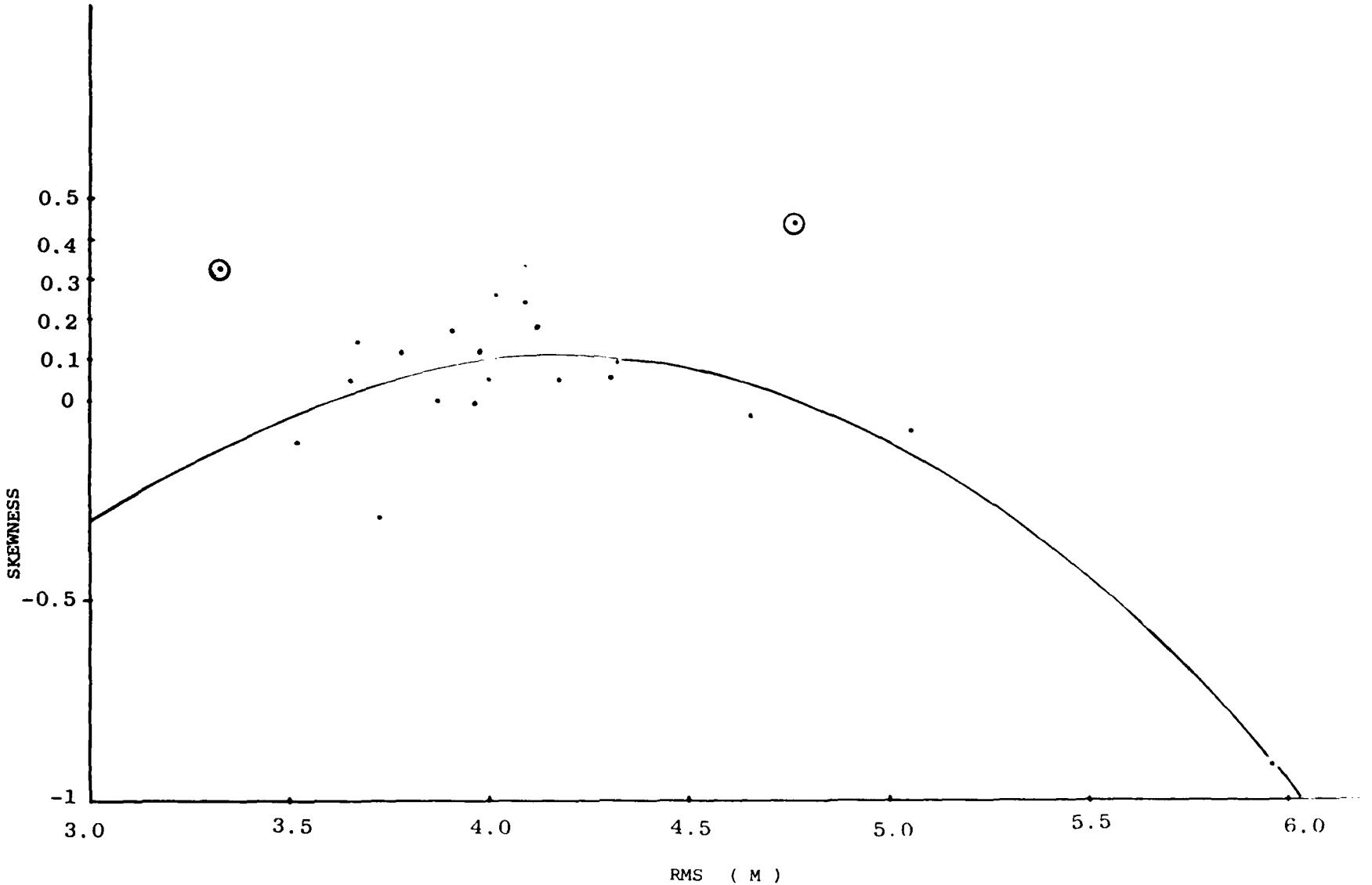

FIGURE 14: A plot of the skewness of VHRR temperature data vs the RMS ice depth for a SW shift to compensate for ice movement can be well fitted by a parabolic curve ($r = 0.89$). Data points with skewness > 0.3 were discarded.

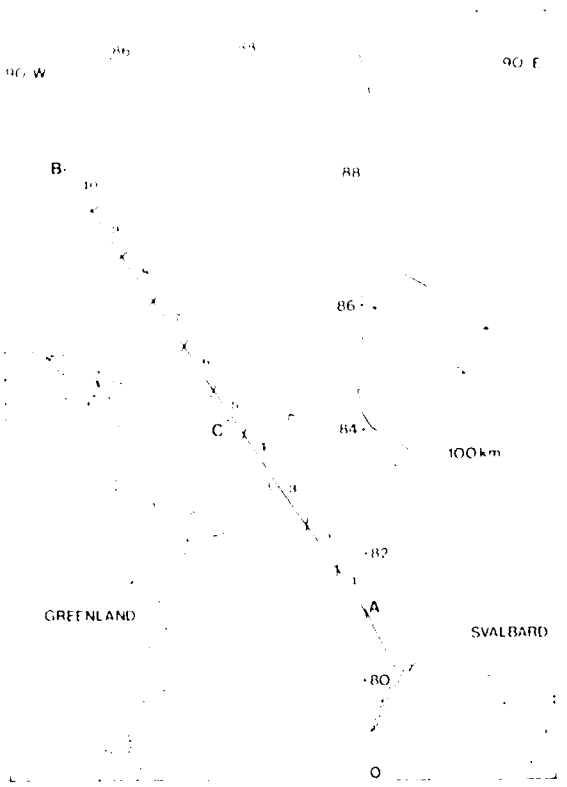

FIGURE 15: Cruise track of HMS SOVEREIGN, October 1976

Wadhams (1978) prepared histograms (probability density functions) of the under-ice depths recorded in each of the 10 97-km zones along Segment AB. These are shown in Figure 16. For each of the 10 zones P(H), the frequency of occurrence, is plotted against the ice depth. In this example, the standard deviation of the mean ice depth was computed from the Wadhams' histograms using the following relationship:

$$\sigma^2 = \left[\frac{f_1 (d_1 - \bar{d})^2 + f_2 (d_2 - \bar{d})^2 + \ldots\ldots + f_n (d_n - \bar{d})^2}{(f_1 + \ldots\ldots f_n - 1)} \right] \qquad (3)$$

where

σ = the standard deviation

f_i = the frequency of occurrence for each 1 m depth cell

d_i = the ice depth at the center point of each 1 m cell

(i.e., $d_1 = 0.5$ m, $d_2 = 1.5$ m, $d_3 = 2.5$ m, etc.)

The computed values for σ are listed in Table 3.

5.2.2 Airborne TIR Data

As shown by LeSchack (1974, 1975, 1976a), when many TIR temperature measurements are made over a sea ice surface, each ice type, i.e., multi-year ice, first-year ice and thin ice, has associated with it a normal or Gaussian distribution of temperatures. For example, if a given ice surface is comprised wholly of multi-year ice, an adequate series of surface temperature measurements produce the familiar "bell-shaped" distribution curve. If there is multi-year and first-year ice in the surface area measured, two slightly overlapping normal distribution curves are produced. When thin ice is also included, three overlapping curves can be seen. The area under each curve is proportional to the amount of surface represented by each type.

In this example, the airborne TIR data were recorded over the submarine track in the form of imagery on 70 mm film. The imagery used was recorded between 1912 hrs and 2040 hrs on 19 October 1976. This section of imagery had been carefully annotated by Dr. Bev Young of the Canadian Department of National Defense and the geographical position of the imagery can be easily ascertained. Between 1912 and 2040 hrs, aircraft altitude was constant, there was no cloud cover, and the IR instrument operator left the gain control constant so that the photographic gray scale, although not temperature-calibrated, maintained the same temperature/gray scale relation-

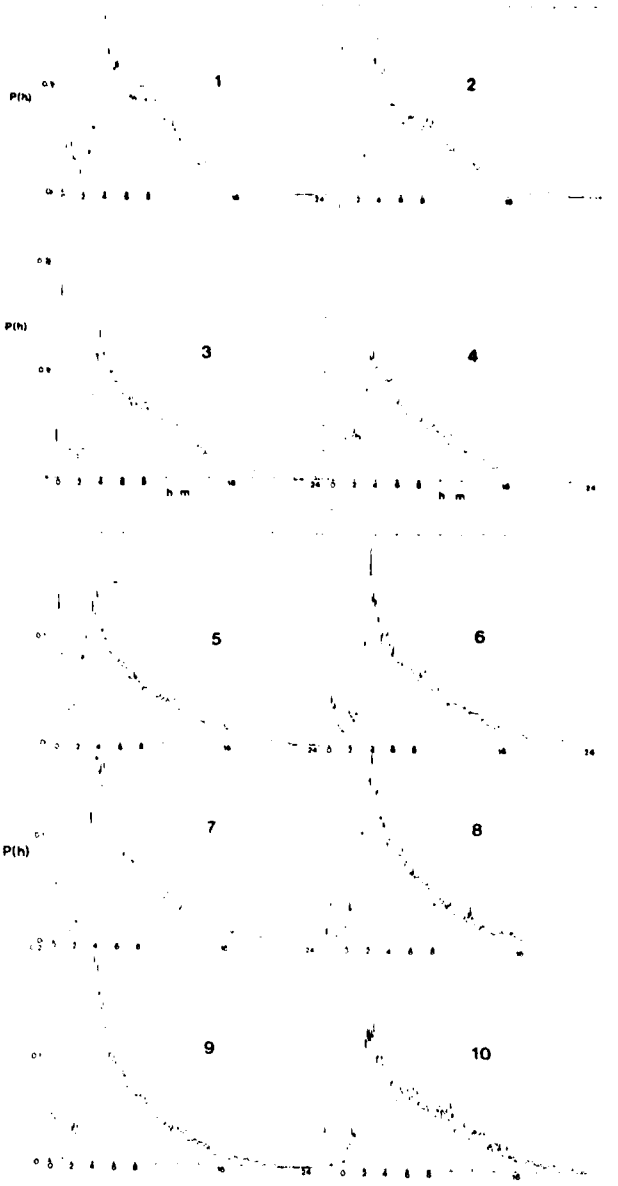

FIGURE 16: Probability density functions of ice draft. Plots are numbered according to divisions seen along Segment AB in Figure 15. (after Wadhams,1978)

ship. During this period, imagery covering sections 4-8 of the submarine track was obtained.

Five sections of imagery, representing the ice surfaces close to the center of each segment, were scanned with a Photometric Data Systems Inc. Series 1000 Microdensitometer[1] to obtain quantitative values proportional to the ice surface temperature. Each area scanned was chosen so that a majority, if not all, of the surface was multi-year ice. The decision was made by photo-interpretive means. A straight scan line 19 cm long through the center of the image, parallel to the line of flight, was made. A circular aperture 86 μm in diameter was used to measure density. A density value was recorded every 86 μm along the scan for a total of 2210 samples per scan.

In the imagery used, the lower the film density, the warmer the surface; hence, the thinner the ice. No functional relationship between the film density and the actual surface temperature is known, since the IR scanner was not calibrated. All that can be said is that the range of thin ice to multi-year ice results in a monotonic increase in film density from approximately 1.0 to 2.0 density units for all five scans. Since this range is typically in the linear portion of the D-log E or Hurter-Driffield curve (for example, see Thompson, 1966, p. 248), it can be assumed that the density/ice thickness relationship is at least constant among the five scans, and this is sufficient to evaluate variations of skewness of the density (or ice thickness) distribution for these five samples.

5.3 Correlation of Under-Ice Roughness with Skewness of Surface Temperature Distribution

Figures 17-21 show positive images of the negative imagery actually scanned for the present analysis. Beneath each image is a histogram of the film density values derived from the scan. Where there is multi-year ice only in the imagery, the histogram of density values suggests a single normal distribution. Overlapping normal distributions can be seen when first-year or thin ice is observed in the imagery.

For this work, only the statistics of the multi-year ice distribution are used. Where there is an overlapping first year distribution, the technique of subtracting the estimated first-year ice histogram from the multi-year histogram is used (see for example, Mack, 1967, p. 140). From the histogram of the multi-year ice, the skewness, s, or the amount that the "bell-shaped" curve leans to the left or the right, was determined as follows:

[1]Courtesy Research Institute, U.S. Army Engineer Topographic Laboratories, Fort Belvoir, Virginia.

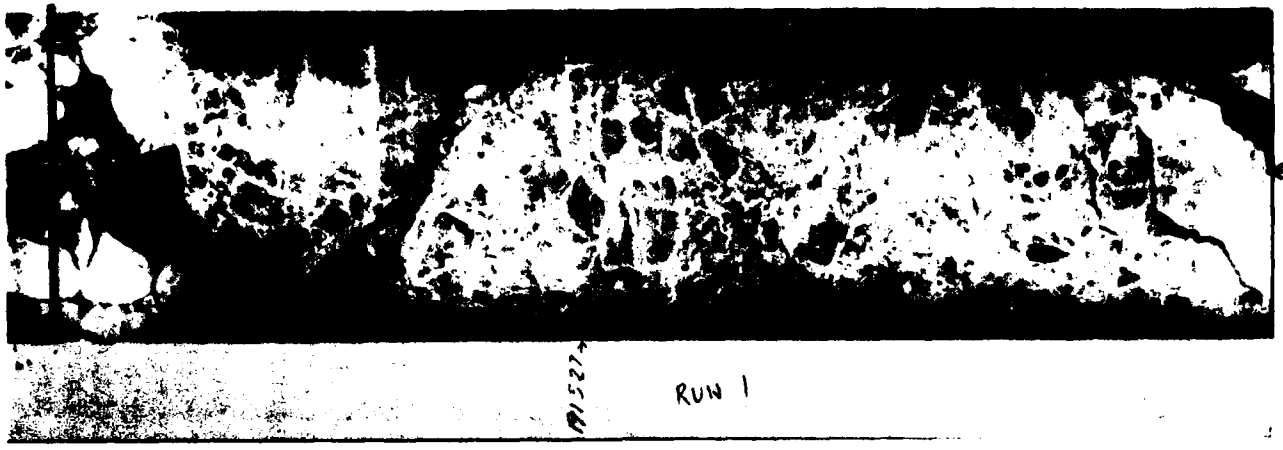

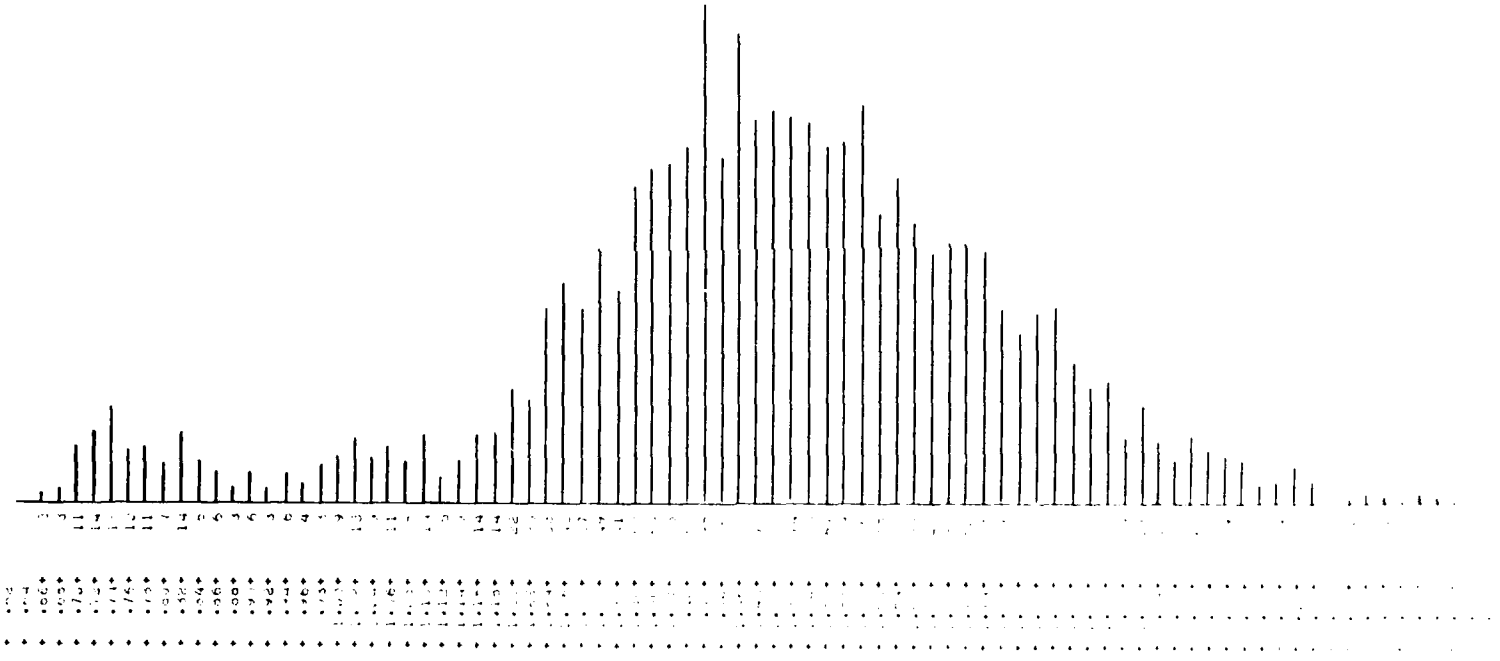

FIGURE 17: TIR image (above) of central portion of region 4 in Segment AB. Approximately 10 km have been covered by the 19 cm microdensitometer scan indicated between the arrows. The histogram of film density values is displayed below. The two minor distributions to the left are associated with thin ice and first-year ice. The major distribution is associated with multi-year ice and has a skewness of -0.475.

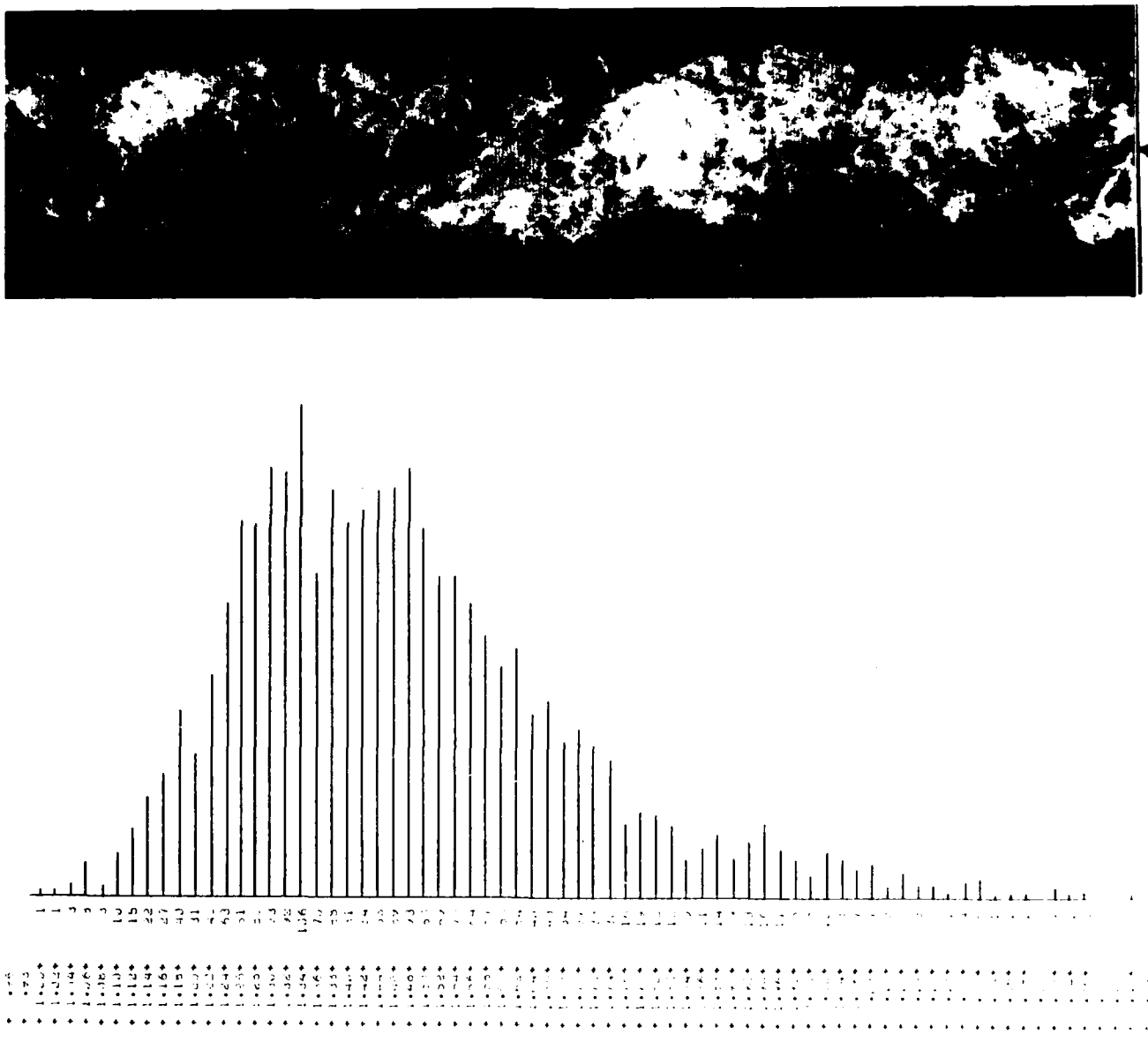

FIGURE 18: TIR image (above) of central portion of region 5 in Segment AB. Approximately 10 km have been covered by the 19 cm microdensitometer scan indicated between the arrows. The histogram of film density values is displayed below. The scan covers all multi-year ice, hence there are no minor distributions. The skewness of the distribution is -0.983.

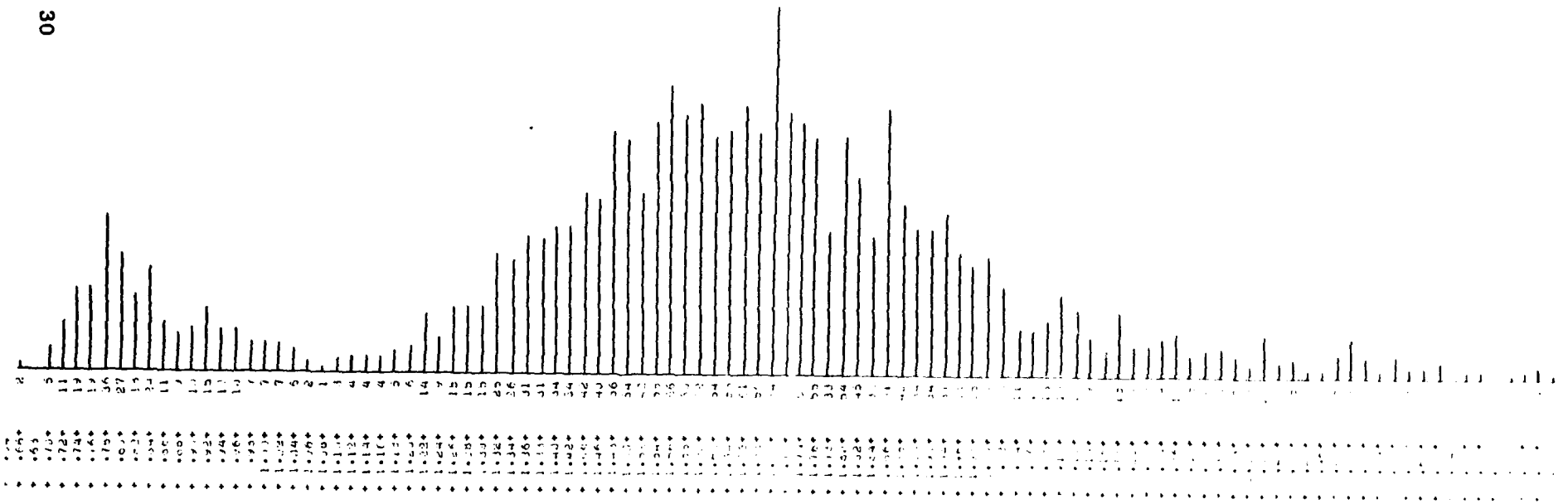

FIGURE 19: TIR image (above) of central portion of region 6 in Segment AB. Approximately 12 km have been covered by the 19 cm microdensitometer scan indicated between the arrows. The histogram of film density values is displayed below. The two minor distributions to the left are associated with thin ice and first-year ice. The major distribution is associated with multi-year ice and has a skewness of -0.830.

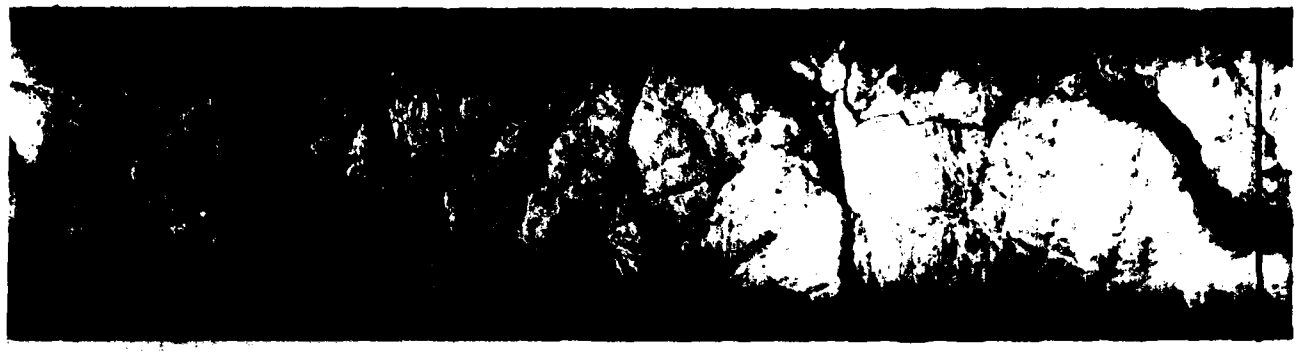

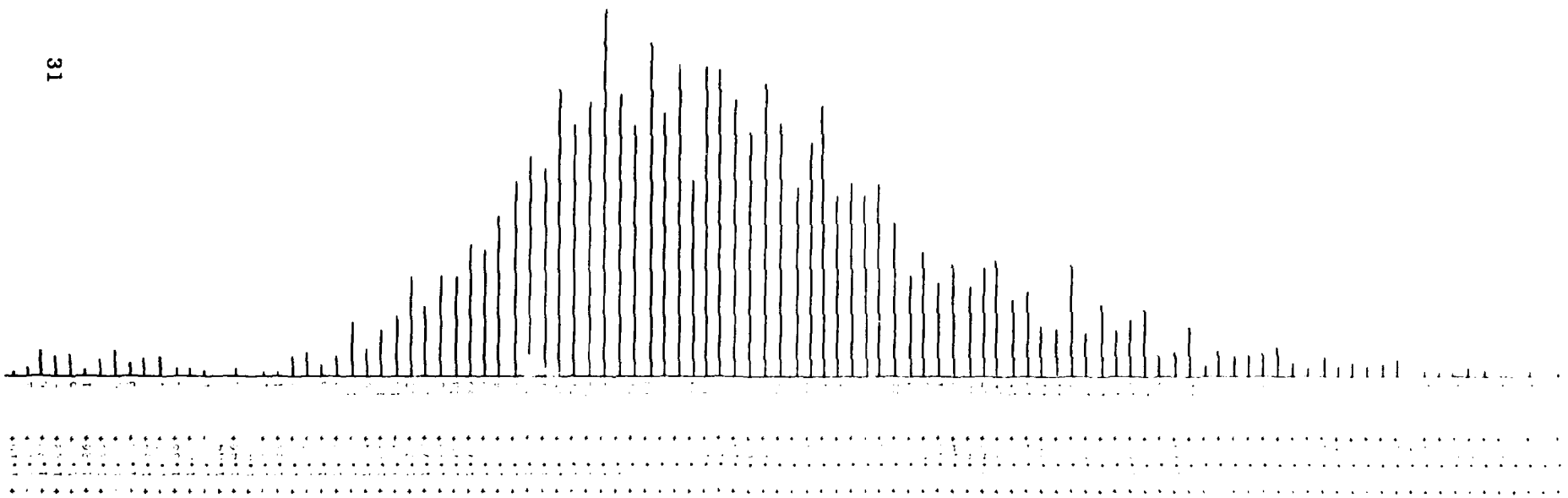

FIGURE 20:TIR image (above) of central portion of region 7 in Segment AB. Approximately 11 km have been covered by the 19 cm microdensitometer scan indicated between the arrows. The histogram of film density values is displayed below. The two minor distributions to the left are associated with thin ice and first-year ice. The major distribution is associated with multi-year ice and has a skewness of -0.713.

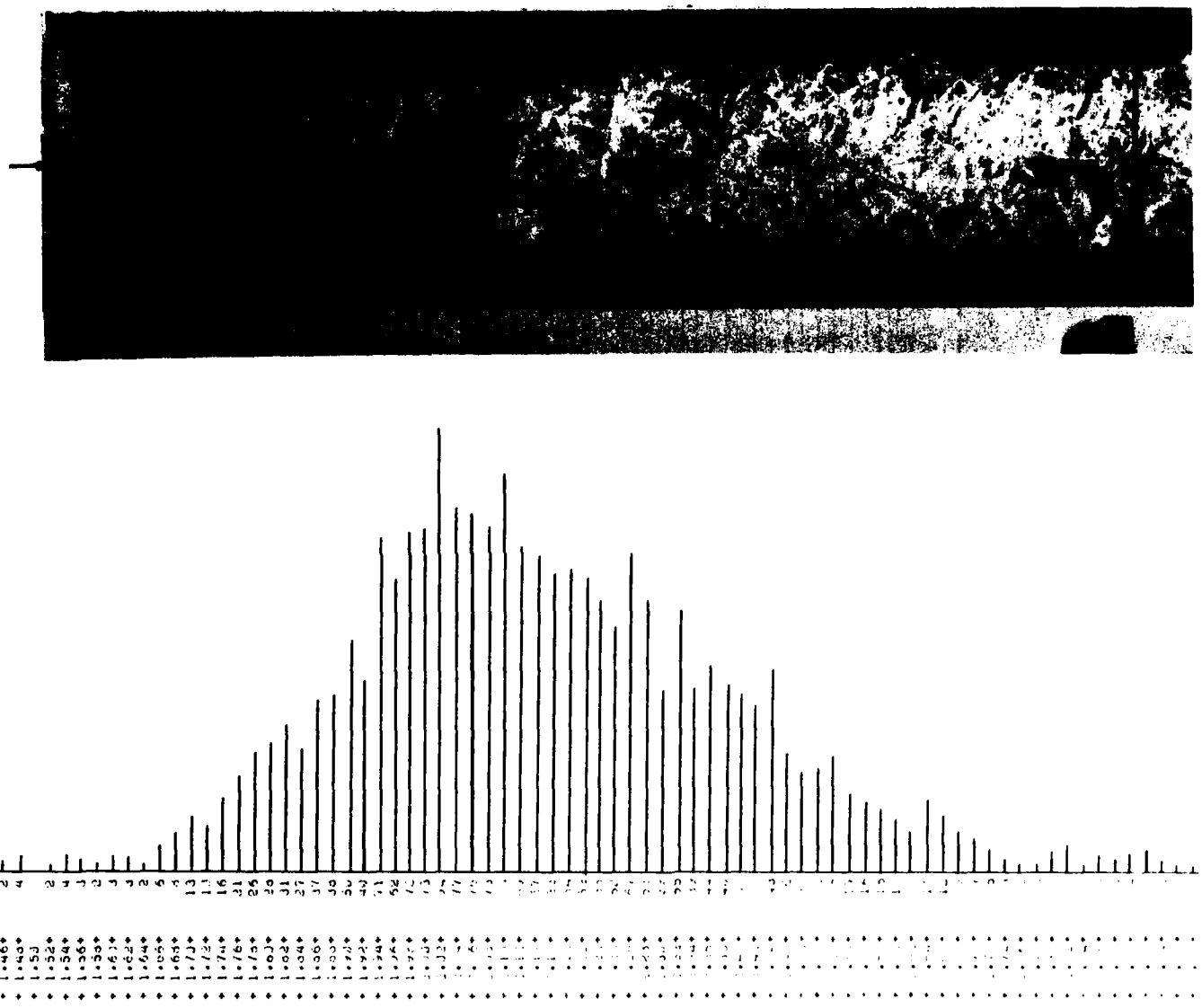

FIGURE 21: TIR image (above) of south-central portion of region 8 in Segment AB. Approximately 11 km have been covered by the 19 cm microdensitometer scan indicated between the arrows. The histogram of film density values is displayed below. The very minor distribution of low density values to the left of the histogram are due to the thin ice and/or first year ice seen at the left of the IR image. The major distribution is associated with multi-year ice and has a skewness of -0.580.

$$S = \left(M_3 / M_2^3\right)^{1/2} \tag{4}$$

and

$$M_r = \left[\frac{F_1 (x_1 - \bar{x})^r + f_2 (x_2 - \bar{x})^r + \ldots\ldots + f_n (x_n - \bar{x})^r}{f_1 + f_2 + \ldots\ldots f_n}\right] \tag{5}$$

where

M_r = the r th moment about the mean

S = skewness

x_i = the film density values (the center of each class interval is chosen)

f_i = the frequency of occurrence of x_i

The values of the skewness as computed from (4) and (5) and from the histograms shown in Figures 17-21 are listed in Table 3. To be consistent with the two examples cited earlier, we are defining positive skewness as: a skewing of the temperature distribution toward higher temperatures, and negative skewness as a skewing toward lower temperatures.

When the values of skewness of the distribution of ice surface temperatures are compared with the measured under-ice roughness, i.e., standard deviation of ice depth, once again a clear functional relationship exists, as shown in Figure 22. The distribution of surface temperature measurements of sea ice skews toward the colder, or thicker ice as deformation increases. In the range of standard deviation of ice depth covered in this example, i.e., between 4.3 and 4.8 m, the relationship is linear and negative.

6. Discussion of the Data

In all three examples, when the RMS ice depth range was between 4 and 8 m, corresponding to a standard deviation of ice depth ranging between 2 and 6 m, there is a strong, negative linear correlation between the skewness of the temperature distributions, whether measured from satellites or aircraft, and the under-ice roughness measured by submarine upward-looking sonar.

Although mathematically a parabola appears to produce the best fit for all the data points used in the example presented in Section 4, the physical significance of a parabolic correlation when the RMS ice depth is less than 4 m (3.5 m mean ice depth) is as yet unknown. Above 4 m RMS ice depth, or 2 m

TABLE 3: Comparison of standard deviation about the mean ice depths for the 10 97-km segments shown in Figure 15 with the skewness of the film density distribution shown in Figures 17-21.

AREA (from Figure 15)	STANDARD DEVIATION (ice, in m)	SKEWNESS (TIR histograms)
1	3.995	
2	4.266	
3	4.557	
4	4.345	-0.475
5	4.783	-0.983
6	4.677	-0.830
7	4.617	-0.713
8	4.554	-0.580
9	4.057	
10	4.735	

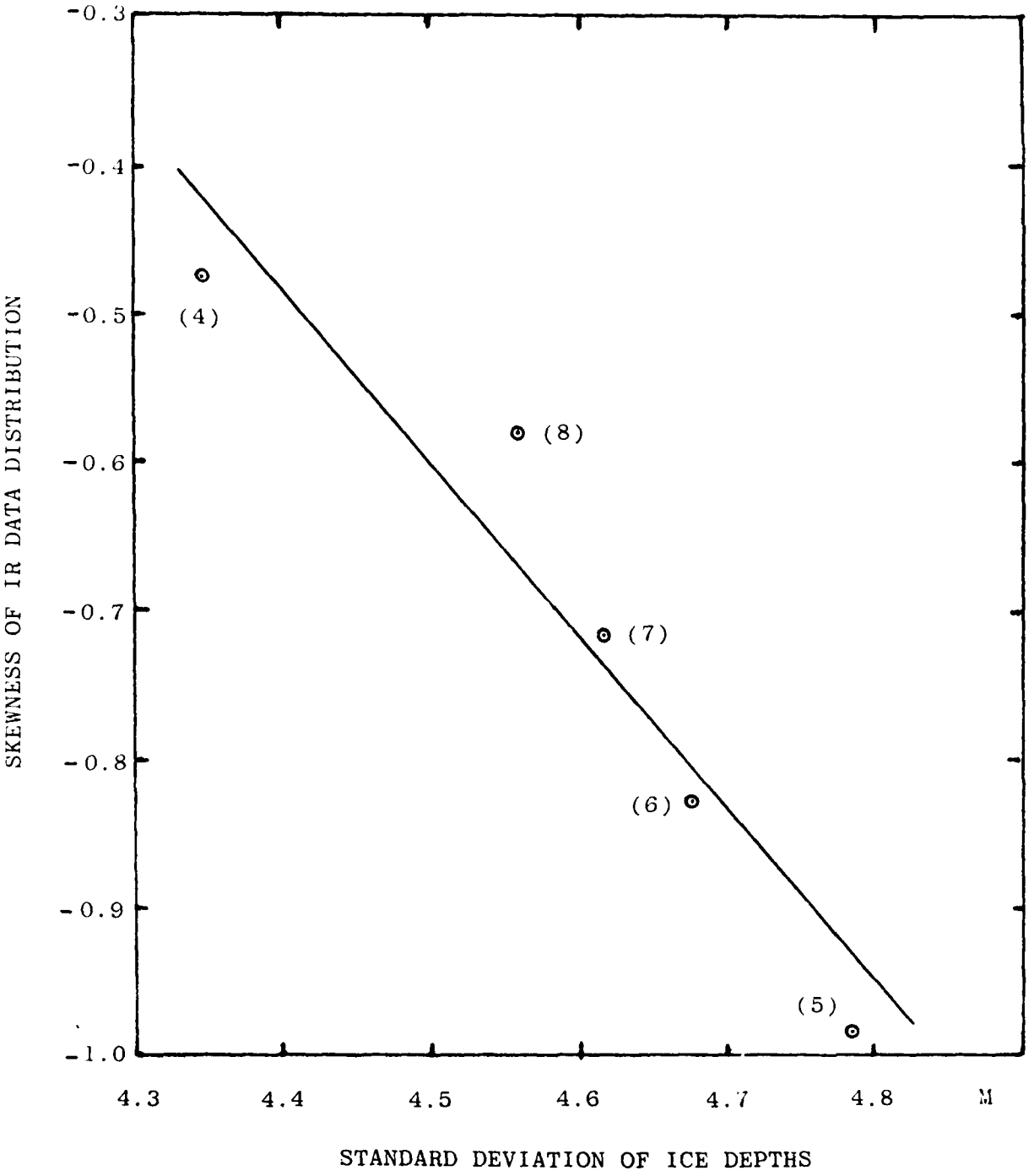

FIGURE 22: Correlation of the skewness of the TIR Temperature distributions with the standard deviations of ice depths for the same regions. The specific regions are noted on the plot.

standard deviation (representing most of the deformed ice in the Arctic), the correlation is simply explained: with increasing ridging, the colder the ice appears relative to the statistical mode of the ice temperature distribution. This portion of the correlation curve is thus consistent with the other analyses shown in Figures 8 and 22. In fact, from 4 m RMS ice depth and deeper, a linear correlation as was used in Figures 8 and 22 can equally well fit the data. It is highly significant that a functional relationship exists between the satellite or airborne TIR and the under-ice roughness data.

As can be seen from Figure 2, most of the SSN GURNARD ice depth data falls between 3.5 and 4.5 m RMS. This is evident in Figure 14 where most of the useable data falls in the region where the slope of the correlation curve is close to zero. In this region, examined with the other data excluded, it is uncertain whether there is real correlation, i.e., is the parabolic function correct, or is there, in fact, no correlation.

Even with the uncertainty of the physical significance of the data in the 3.5-4.0 m RMS ice depth region it is clear that statistically, the chances are excellent that there is a relationship between the skewness of the satellite TIR data and the RMS under-ice roughness data. Such directional correlations, consistent with the actual ice drift, are highly unlikely to occur by chance. In view of all of the above, it must be concluded that the first set of correlations observed with the SSN SARGO data taken in 1960 and satellite data taken in 1974 were not an accident; there appears to be a real correlation that has important ramifications for predicting under ice roughness for acoustic propagation in the Arctic.

7. Conclusions

Although different units of measurement, as dictated by the three available data sets, were used in the correlations to date, one thing is clear from the data presented here. For under ice roughness measured in terms of RMS ice depth between the ranges of 4 m and 8 m, or in terms of standard deviation about the mean in ranges of 2 m and 6 m, there is a good negative linear correlation with the skewness of the temperature distribution of the corresponding ice surface, where increasing negative skewness is defined as the temperature measurements skewing toward lower temperatures.

Experimental evidence reveals a definite relationship. To define the relationship numerically, the parameters being correlated must be expressed consistently. This is easily done with the under-ice parameter which is measured in a straightforward manner, and can be expressed as standard deviation or RMS ice depth, and appears conservative over time (LeSchack and Chang 1977).

On the other hand, the skewness of the surface temperature distribution, which appears to be the most sensitive measurement of variations in ice surface roughness found, has a numerical range that varies with the number of measurements used in its determination and most probably, the time of year the measurements were made. As a result, it is likely that a given under-ice roughness predictive equation must be developed from TIR data recorded at essentially the same time.

It is concluded that the under ice roughness of multi-year ice may be predicted from airborne or satellite TIR measurements. An universal predictive equation has yet to be developed, however, since sufficient data are not presently available.

8. References

Buck, B.M., (1975) Personal Communication, Polar Research Laboratories, Santa Barbara, CA 93101.

Buck, B.M., (1977) Personal Communication, *ibid*

Buck, B.M., (1979) Personal Communication, *ibid*

Barnett, T.P., (1966) A Scheme for Determining the Two-Dimensional Roughness Characteristics of an Icepack, U.S. Navy Journal of Underwater Acoustics, V16, N2 (U).

Dunbar, M. and Wittman, W. (1973) Some Features of Ice Movement in the Arctic Basin, Proc. of Arctic Basin Symp., Arctic Inst. of North America, Arlington, Va., pp 90-108.

Hibler, W.D. III, Mock, S.J. and Tucker, W.B., III, (1974), Classification and Variation of Sea Ice Ridging in the Western Arctic Basin, J. Geophys. Res, V79, N18, pp 2735-2743.

LeSchack, L.A., (1974) Potential Use of Satellite Infrared Data for Ice Thickness Mapping, The Coast and Shelf of the Beaufort Sea, J.C. Reed and J.E. Sater, eds., Arctic Inst. of North Amer., Arlington, Va., pp 243-267..

LeSchack, L.A., (1975) Potential Use of Satellite IR Data for Ice Thickness Mapping, Final Report, NOAA/NESS Contract 3-35384, Development and Resources Transportation Company, Silver Spring, Maryland 20902.

LeSchack, L.A., (1976a) Potential Use of Satellite IR Data for Ice Thickness Mapping, Appendix to Final Report (Contract 3-35384) NOAA/NESS Contract 5-35403, Development & Resources Transportation Co., Silver Spring, Md. 20902.

LeSchack, L.A., (1976b) Applications of Submarine Under-Ice Profiles and Satellite IR Data to Solving Arctic Offshore Problems, Proc. 3rd Int'l Conf. on Port and Ocean Engineering Under Arctic Conditions, 11-15 Aug 1975, U. of Alaska, Inst. of Mar. Sci., pp 141-162.

LeSchack, L.A. and Chang, D.C., (1977) Arctic Under-Ice Roughness, Tech Rept for ONR Contract N00014-76-C-0757/NR 307-304, Development & Resources Transportation Co., Silver Spring, Md. 20902.

Lyon, Waldo K. (1963), The Submarine and the Arctic Ocean, Polar Record, 11:75 (699-705).

Mack, C., (1967) Essentials of Statistics for Scientists and Technologists, Plenum Press, New York.

Maykut, G.A. and Untersteiner, N. (1971), Some Results from a Time-Dependent Thermodynamic Model of Sea Ice, J. Geophs. Res. V76, N6, pp 1440-75.

Thompson, M.M. ed., (1966) Manual of Photogrammetry, 3rd ed. Amer. Soc. of Photogrammetry, Falls Church, Va 22044.

Thorndike, A.S. and Cheung, J.Y. (1977) Aidjex Measurements of Sea Ice Motion 11 April 1975 to 14 May 1976, AIDJEX Bulletin N35.

Wadhams, P., 1978, A Comparison of Sonar and Laser Profiles along Corresponding Tracks in the Arctic Ocean, unpublished manuscript, Scott Polar Research Inst., Cambridge, England.

9. Acknowledgement

Much of the numerical analysis of the satellite data discussed in this report was conducted under National Oceanic and Atmospheric Administration Contracts 3-35384, 5-35403 and 7-35173. The assistance of Dr. E. Paul McClain and Mr. John Pritchard of this agency is gratefully acknowledged. Drs. Waldo K. Lyon of the Naval Ocean Systems Center's Arctic Submarine Laboratory and Huon Li of the Naval Ocean Research and Development Activity are the sources of the data recorded by U.S. nuclear submarines, as well as much valuable assistance. The airborne TIR data were provided by Dr. Bev Young of the Canadian Defense Research Establishment in Ottawa, and the HMS SOVEREIGN under-ice data were provided by Dr. Peter Wadhams of the Scott Polar Research Institute, Cambridge, England.

APPENDIX A

Statistical Analysis of the VHRR TIR Satellite Data

The satellite TIR data is broken up into basic 32 x 32 km arrays as seen in Figure 6. Each 32 x 32 array is composed of 1024 measurements of radiant temperature (in the 16 x 16 km arrays used in Section 4 of the report, 256 measurements are contained). Like many measurements, the temperature measurements of multi-year ice appear to fall into a Gaussian, or normal distribution. Mathematically we can express deviations from the familiar "bell-shaped" curve by skewness (whether the bell leans to the left or the right) and by kurtosis, the peakedness of the curve. These terms are expressed as follows:

$$S = M_3/(M_2^3)^{1/2}$$

$$k = M_4/M_2^2$$

and

$$M_r = \frac{f_1(X_1-M)^r + f_2(X_2-M)^r + \ldots + f_N(X_N-M)^r}{f_1 + f_2 + \ldots + f_N}$$

where

M_r = the r th moment about the mean; M = the mean

S = skewness

K = kurtosis

X_i = the radiant temperature values

f_i = the frequency of occurrence of X_i

N = the total number of values per matrix

APPENDIX B

SURFACE TEMPERATURE DISTRIBUTION STATISTICS FOR NOAA VHRR SATELLITE REV 6000, 8 MARCH 1976 OVER AIDJEX TRACK

No.	NOAA LINE	ID SPOT	MEAN COUNT[1]	STD. DEV.	SKEWNESS	KURTOSIS	ESTIMATED ICE TYPE[2]	No.	NOAA LINE	ID SPOT	MEAN COUNT[1]	STD. DEV.	SKEWNESS	KURTOSIS	ESTIMATED ICE TYPE[2]
1	2416	2452	70.65	3.01	0.63	3.85	.9 M, .1F	30	2512	2836	72.56	2.10	0.26	2.57	M
2	2416	2476	71.32	3.12	0.32	2.59	.9 M, .1F	31	2528	2644	72.65	3.02	1.00	5.27	.9 M, .1F
3	2416	2500	71.64	4.21	1.29	5.83	.8 M, .2F	32	2528	2812	72.56	2.20	-0.29	3.44	M
4	2416	2524	73.06	5.24	0.88	3.32	.7 M, .3F	33	2544	2668	73.36	3.40	1.16	5.08	.9 M, .1F
5	2416	2548	71.50	4.00	1.80	8.32	.9 M, .1F	34	2544	2788	72.45	3.10	1.80	10.72	M, trace F
6	2416	2572	71.11	3.00	0.24	2.20	M	35	2560	2692	72.25	2.63	0.08	2.94	M
7	2416	2596	71.45	3.03	0.44	2.77	M	36	2560	2764	74.91	4.31	2.02	8.23	.9 M, .1F
8	2432	2476	71.37	2.24	0.0	2.59	M	37	2576	2716	73.48	2.15	0.05	2.53	M
9	2432	2500	72.37	3.18	1.28	7.65	.95 M, .05F	38	2576	2740	73.63	2.29	0.09	2.97	M
10	2432	2644	72.46	3.28	1.95	8.47	.90 M, .1F	39	2592	2692	73.29	2.36	0.51	3.48	.95 M, .05F
11	2432	2668	73.87	4.16	1.31	4.76	.8 M, .2F	40	2592	2716	73.95	2.90	0.99	4.26	.9 M, .1F
12	2432	2692	70.56	2.93	1.28	6.94	.95 M, .05F	41	2592	2740	74.41	2.55	0.60	3.77	.95 M, .05F
13	2432	2716	71.46	2.75	1.25	5.59	.9 M, .1F	42	2608	2668	74.86	2.81	0.46	3.71	.95 M, .05F
14	2432	2740	71.34	2.30	0.0	3.19	M	43	2608	2764	76.48	4.11	1.85	7.37	.9 M, .1F
15	2432	2764	73.03	4.41	1.72	6.47	.8 M, .2F	44	2624	2644	75.41	3.96	1.16	4.10	.95 M, .05F
16	2432	2788	71.47	2.43	0.05	2.68	M	45	2624	2788	75.08	2.21	0.05	2.99	M
17	2432	2812	71.47	2.20	0.12	2.68	M	46	2640	2596	76.61	2.64	0.52	3.97	.95 M, .05F
18	2432	2836	71.99	3.00	1.43	6.52	.95 M, .05F	47	2640	2620	76.96	2.66	0.53	3.12	.9 M, .1F
19	2432	2860	70.77	2.22	-0.11	2.78	M	48	2640	2812	76.56	1.87	0.18	2.90	M
20	2432	2884	70.74	2.71	0.35	3.65	.95 M, .05F	49	2656	2572	75.47	2.41	-0.08	3.04	M
21	2432	2908	72.92	3.08	0.79	4.84	.85 M, .15F	50	2656	2836	72.93	4.20	1.32	4.66	.8 M, .2F
22	2448	2932	73.08	2.66	0.13	3.49	.8 M, .2F	51	2672	2548	77.37	4.15	1.53	5.77	.75 M, .25F
23	2448	2548	71.09	2.60	0.05	2.90	M	52	2672	2860	79.81	3.60	0.67	3.36	.85 M, .15F
24	2464	2908	72.84	3.77	1.17	4.48	.9 M,	53	2688	2524	75.72	2.43	-0.91	4.91	M
25	2480	2572	72.77	2.87	0.12	2.83	M	54	2688	2884	80.10	3.61	1.52	6.26	.75 M, .25F
26	2480	2884	74.61	4.21	1.19	5.10	.75 M, .25F	55	2704	2500	75.86	2.43	-0.04	2.66	M
27	2496	2596	71.23	2.39	0.14	2.88	M	56	2704	2908	81.39	3.19	1.03	4.51	.9 M, .1F
28	2496	2860	72.09	3.20	1.55	7.97	.95 M, .05F	57	2720	2476	76.10	2.10	0.17	3.15	M
29	2512	2620	71.40	2.37	0.33	4.10	M	58	2720	2932	83.73	6.48	0.97	2.98	.60 M, .4F

[1]Mean count is proportional to temperature. A count of 1 is approximately equal to $1^{o}C$.

[2]Fraction of ice type is estimated by photo interpretation of the VHRR TIR imagery. M = multi-year ice; F = first-year ice.

UNCLASSIFIED
Security Classification

AD-A085 512

DOCUMENT CONTROL DATA - R & D

(Security classification of title, body of abstract and indexing annotation must be entered when the overall report is classified)

1. ORIGINATING ACTIVITY (Corporate author)	2a. REPORT SECURITY CLASSIFICATION
LeSchack Associates, Ltd. 1111 University Blvd. West Silver Spring, Maryland 20902	UNCLASSIFIED
	2b. GROUP

3. REPORT TITLE

CORRELATION OF UNDER-ICE ROUGHNESS WITH SATELLITE AND AIRBORNE THERMAL INFRARED DATA

4. DESCRIPTIVE NOTES (Type of report and inclusive dates)
Technical Report

5. AUTHOR(S) (First name, middle initial, last name)

Leonard A. LeSchack

6. REPORT DATE	7a. TOTAL NO. OF PAGES	7b. NO. OF REFS
May 1980	42	17

8a. CONTRACT OR GRANT NO.	9a. ORIGINATOR'S REPORT NUMBER(S)
N00014-76-C-0757	
b. PROJECT NO. NR 307-374	0757-2
c.	9b. OTHER REPORT NO(S) (Any other numbers that may be assigned this report) N/A
d.	

10. DISTRIBUTION STATEMENT

Distribution of this document is unlimited

11. SUPPLEMENTARY NOTES	12. SPONSORING MILITARY ACTIVITY
	Office of Naval Research 800 N. Quincy Street Arlington, Virginia 22217

13. ABSTRACT This report, based on empirical data, concludes that a correlation has been found between easily obtainable sea ice surface temperature and under-ice roughness data which are obtainable only at great expense. Under-ice roughness is valuable in evaluating acoustic attenuation beneath the Arctic ice and is expressed in terms of either root-mean-square (RMS) ice depth or standard deviation about the mean ice depth, both of which are closely correlated. By showing a functional relationship between the skewness of the surface temperature distribution as derived from NOAA VHRR Satellite thermal infrared data and the under-ice roughness, the way appears clear to make a chart of Arctic under-ice roughness for Arctic acoustic programs and for nuclear submariners.

Specifically, a comparison of the skewness of the temperature distribution derived from NOAA VHRR thermal infrared satellite data of the Beaufort Sea taken in April 1974 was made with the RMS under-ice roughness derived from under-ice profile data recorded by the SSN SARGO in February 1960 taken at essentially the same locations. Five data sets were chosen ranging from the highly deformed and hence thicker ice area near the Canadian Archipelago to thinner ice off the coast of Alaska near Prudhoe Bay. A very high negative correlation was observed.

In a second study, under ice data recorded in April 1976 by the SSN GURNARD was correlated with the skewness of temperature distributions derived from NOAA VHRR IR data recorded in March 1976 over nominally the same area of the Beaufort Sea. The SSN GURNARD cruise track of some 780 N. miles was divided into 63, 10 N. mile (16 km) sections. The NOAA VHRR IR data were similarly grouped into 10 N. mile squares that nominally corresponded to the positions from where RMS under ice data were gathered.

DD FORM 1 NOV 68 1473 REPLACES DD FORM 1473, 1 JAN 64, WHICH IS OBSOLETE FOR ARMY USE.

UNCLASSIFIED
Security Classification

14 KEY WORDS	LINK A		LINK B		LINK C	
	ROLE	WT	ROLE	WT	ROLE	WT
Under Ice Roughness						
Airborne and Satellite IR Scanning						
Sea Ice Measurements						
Remote Sensing						

ABSTRACT continued

Twenty useable skewness values were obtained with the RMS under ice data. Because of the relatively high resolution, i.e., 10 N. miles, some data set misregistration was anticipated, but by moving the satellite data matrix about 10 NM to the west, northwest or southwest, a good registration was found and a good statistical correlation was obtained. This slight matrix shifting appears significant because it is consistent in both direction and magnitude with the actual measured ice drift between March and April 1976. Also, shifting in any of the other three quadrants shows no correlation.

A third study was then conducted that shows, perhaps more graphically than the others, the correlation of under-ice data recorded by the British nuclear submarine HMS SOVEREIGN between 18-21 October 1976 with airborne IR data recorded during the same period over the submarine track by a Canadian Forces Argus aircraft. The airborne IR data are recorded in the form of imagery on a scale large enough to see the individual features of the ice surface. A scanning microdensitometer generated histograms of film density values that are proportional to ice surface temperatures. The skewness of the histograms were correlated with the standard deviations about the mean ice depth for the associated submarine track.

In all three examples, when the RMS ice depth range was between 4 and 8 m, corresponding to a standard deviation of ice depth ranging between 2 and 6 m, there is a strong, negative linear correlation between the skewness of the temperature distributions, whether measured from satellites or aircraft, and the under-ice roughness measured by submarine upward-looking sonar.